https://doi.org/10.1016/j.tws.2022.110515

Cyclic compressive behavior and load-strain model of FRP-concrete double tube composite columns

Shuai Li Tak-Ming Chan* Ben Young

Department of Civil and Environmental Engineering, The Hong Kong Polytechnic University, Hong Kong, China

*Corresponding author. *Email address:* tak-ming.chan@polyu.edu.hk (T.-M. Chan).

Abstract

A novel fiber-reinforced polymer (FRP) – concrete double tube composite column, consisting of an outer filament winding FRP tube, an inner pultruded FRP tube and infilled core concrete and ring concrete, has been proposed and experimentally investigated under monotonic compression by the authors. It exhibited obviously improved deformability than the traditional FRP-confined concrete columns. In this study, cyclic compression tests were conducted on the composite column to examine its structural behavior under cyclic loadings. Effects of different outer and inner FRP tube thicknesses and ring concrete types were investigated. Failure modes, cyclic load-strain responses and hoop strain behavior were presented and analyzed. Cyclic load-strain model, including the envelope model, unloading and reloading models, plastic strain equation and stress deterioration equation, was proposed to predict the cyclic compressive behavior of the FRP-concrete double tube composite columns. The proposed model was verified against the test results and exhibited good performance.

Keywords: Cyclic compression; Cyclic load-strain model; Double tube; FRP-concrete; Hoop strain; Ultimate axial strain

1. Introduction

Fiber-reinforced polymer (FRP) – confined concrete column is an effective structural form that has been widely investigated and adopted in engineering practice [1-4]. With the FRP confinement, both the compressive strength and strain of concrete can be significantly enhanced [5-8]. Various composite columns based on the FRP-confined concrete column have been developed in recent years, such as the FRP-confined concrete filled steel tube (CFST) columns [9,10], FRP-concrete-steel double skin tubular columns (DSTCs) [11,12] and double tube concrete columns (DTCCs) [13,14]. Better ductility performance can be achieved when steel is used in these composite columns [15,16]. Meanwhile, advanced concrete materials including ultra-high performance concrete (UHPC) and fiber-reinforced concrete have also been explored in FRP-confined concrete system to further improve the

structural behavior of the columns [17-20]. A novel FRP-concrete double tube composite column was proposed and experimentally investigated by the authors recently [21]. It consists of an outer filament winding FRP tube, an inner pultruded FRP tube and infilled core concrete and ring concrete as shown in Fig. 1. It was developed on the basis of the traditional solid FRP-confined concrete column and aimed to achieve enhanced structural performance. High strength concrete (HSC) was adopted in the core region to obtain higher compressive capacity, while less brittle concrete like normal concrete (NC) with medium compressive strength or engineered cementitious composite (ECC) was adopted in the ring region to ease the column brittleness and improve the column deformability. It was observed that the FRP-concrete double tube composite column could achieve higher FRP confining efficiency and delayed column failure, with obviously improved deformability than the corresponding traditional FRP-confined HSC columns [21]. The inner pultruded FRP tube can contribute to the axial load capacity and serve as longitudinal reinforcement to provide bending resistance under eccentric compression. Compared with the aforementioned FRP-concrete-steel composite columns, this newly proposed composite column is steel-free and could be used in marine environments or used together with seawater sea sand concrete without the concern of steel corrosion problem [22,23]. On the other hand, connection of the proposed composite column could be quite different from the FRP-concrete-steel composite columns, without the convenient connection provided by steel tube. The lower and upper inner pultruded FRP tubes can be firstly aligned in the correct position, followed by the wrapping of FRP jackets near the interface of the two tubes. Additional reinforcements, like FRP plates and FRP rebars, can be attached on the surface of the pultruded FRP tubes and across the interface of the lower and upper tubes for strengthening. For the outer filament winding FRP tube, the similar procedures can be adopted for the connection of the lower and upper tubes, to ensure lateral confinement effectiveness is not reduced in the joint region. After connecting the inner and outer tubes to form the mould, concrete can be cast into the core region and ring region. If incoming beams are considered in the horizontal direction, openings can be left in the corresponding locations of the inner and outer tubes to allow the beam to pass through. In actual engineering, however, the most potential application of this composite column is to be used as bridge pier, where column-column and beam-column connections are not needed. Meanwhile, two different types of concrete in the core and ring regions may bring extra complexity to construction of the composite column. In engineering projects, inner and outer tubes can be assembled to form the mould, followed by the casting of ring concrete in the factory, to firstly form the section of outer filament winding FRP tube – ECC or NC ring – inner pultruded FRP tube, which

can be regarded as a prefabricated composite tube. Then the prefabricated composite tube can be transported to the construction site for the casting of inner HSC core, to form the proposed double tube composite column. With this approach, the construction process of the proposed composite column can be simplified.

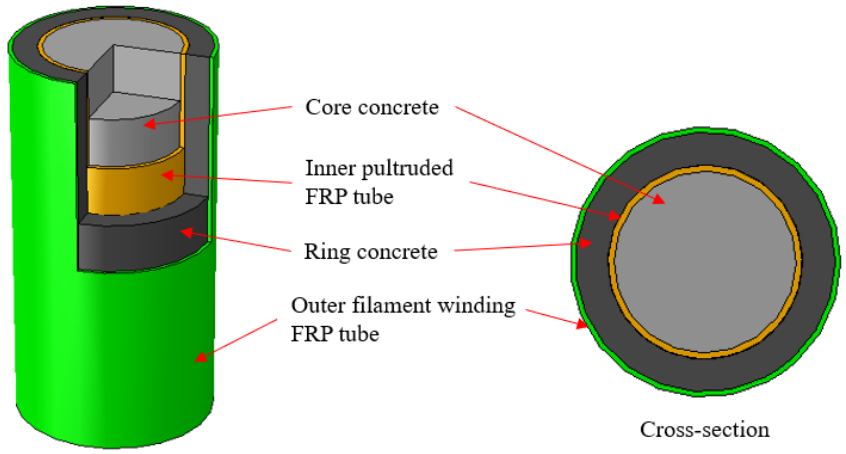

Fig. 1 FRP-concrete double tube composite column

Understanding cyclic compressive behavior of FRP-confined concrete is of vital importance to seismic retrofitting of concrete columns. Extensive studies ranging from experimental investigation to theoretical modeling have been carried out to illustrate the hysteresis behavior of FRP-confined concrete under cyclic compression [24-26]. Shao et al. [27] conducted tests on FRP-wrapped concrete stub columns and proposed the first cyclic stress-strain model. Lam et al. [28] evaluated the model and found that it could not provide accurate predictions on the unloading path. Subsequently, Lam and Teng [29] developed a widely accepted cyclic model that could describe the different components in the cyclic loading process, including the unloading and reloading responses, as well as the plastic strain and stress deterioration caused by the cumulative effect during the repeated loading cycles. It was also noted that the envelope curves for cyclically loaded columns were close to the stress-strain curves for monotonically loaded columns [29]. Yu et al. [30], Wang et al. [31] and Hany et al. [32] further examined the cyclic compressive behavior of FRP-confined concrete columns with higher concrete strengths, larger column size and non-circular sections. Cyclic models with new equations to predict the different cyclic components were also proposed [30-32]. Li et al. [33] additionally considered the confinement rigidity effect on the hysteresis behavior and developed the model that could predict the cyclic compressive behavior including both post-peak hardening and softening. Meanwhile, with the development of various FRP-concrete-steel composite columns in recent years, advanced cyclic stress-strain models considering the dual confinements of FRP and steel have also been proposed [34-36].

When it comes to FRP-confined double tube composite columns [13-16], only Zeng et al. [15] experimentally investigated the double tube composite column (with steel tube as the inner tube) under cyclic axial compression, while the cyclic modeling was not included. Since the proposed FRP-concrete double tube composite column has the potential to be used under seismic loading conditions where columns are required to withstand relatively large deformations, it is important to understand its cyclic compressive behavior and establish the corresponding cyclic model.

In this study, cyclic compression tests were carried out on the FRP-concrete double tube composite column. Failure modes, cyclic load and strain responses were presented and analyzed through the comparison with the corresponding monotonic compressive behavior. Cyclic load-strain model, which was developed based on the cyclic stress-strain models of FRP-confined core concrete and ring concrete, was also proposed to predict the cyclic compressive behavior of the composite column.

2. Experimental investigation

2.1 Test specimens

A total of 28 specimens were included in the test program, in which 16 specimens were tested under monotonic compression and were firstly reported in Li et al. [21], while 12 specimens were newly tested under cyclic compression which is the main focus of this study. All the specimens had the nominal diameter of 200 mm and nominal height of 400 mm. Outer diameter of the inner tube is 150 mm and thickness of the ring concrete is 25 mm for the composite columns. Except for the FRP-concrete double tube composite columns, corresponding traditional FRP-confined HSC columns were also tested for comparison purposes. Test variables, including outer filament winding FRP tube thickness, inner pultruded FRP tube thickness and ring concrete type (i.e. NC or ECC), were investigated in the study. All the tested specimens are listed in Table 1. For specimen label, “F7” or “F10” refers to the outer filament winding FRP tube with 7 or 10 layers of fibers, which is designed to yield different levels of confinement on inner concrete; “PF4” or “PF9” refers to the inner pultruded FRP tube with the nominal thickness of 4 mm or 9 mm, which is designed to contribute different levels of axial load to the composite column; “N” or “E” refers to the NC or ECC used for the ring concrete; “H” refers to the HSC core; “M” or “C” refers to the monotonic or cyclic loading. “R” refers to the repeated test specimen. Taking “F10-E-PF9-H-C” as an example, it refers to the specimen of the FRP-concrete double tube composite column with 10-layer outer filament winding

FRP tube and 9.0 mm-thick inner pultruded FRP tube, as well as ECC as ring concrete and HSC as core concrete under cyclic compression. Specimen preparation process of the composite columns is the same as that presented in Li et al. [21].

Table 1 Specimen label and key test results

Specimen label	F_1 (kN)	ε_{c1}	F_2 (kN)	ε_{c2}	F_c (kN)	ε_{cu}	F_{max} (kN)	$\varepsilon_{c,max}$	$\varepsilon_{h,rup}$
F7-H-M[a]	-	-	-	-	3086.6	0.0118	3365.9	0.0034	0.0110
F7-H-M-R[a]	-	-	-	-	3093.7	0.0127	3366.8	0.0036	0.0112
F7-H-C	-	-	-	-	2863.2	0.0141	3427.1	0.0035	0.0124
F10-H-M[a]					3613.7	0.0135	3613.7	0.0135	0.0121
F10-H-M-R[a]	-	-	-	-	3729.7	0.0130	3729.7	0.0130	0.0117
F10-H-C	-	-	-	-	3563.2	0.0133	3357.6	0.0040	0.0114
F10-H-C-R	-	-	-	-	3625.8	0.0149	3494.1	0.0038	0.0127
F7-N-PF4-H-M[a]	3099.7	0.0107	3065.4	0.0114	3156.9	0.0156	3156.9	0.0156	0.0128
F7-N-PF4-H-C	-	-	-	-	3181.8	0.0156	3181.8	0.0156	0.0118
F7-N-PF9-H-M[a]	3669.1	0.0086	3328.3	0.0119	3385.5	0.0146	3669.1	0.0086	0.0115
F7-N-PF9-H-C	4007.6	0.0098	3917.2	0.0117	3897.5	0.0181	4007.6	0.0098	0.0121
F7-E-PF4-H-M[a]	2535.3	0.0090	2499.7	0.0104	2746.3	0.0155	2746.3	0.0155	0.0113
F7-E-PF4-H-M-R[a]	2479.7	0.0087	2381.2	0.0098	2827.4	0.0169	2827.4	0.0169	0.0111
F7-E-PF4-H-C	-	-	-	-	2894.8	0.0167	2894.8	0.0167	0.0117
F7-E-PF9-H-M[a]	2968.5	0.0091	2738.3	0.0115	2925.2	0.0155	2968.5	0.0091	0.0092
F7-E-PF9-H-M-R[a]	3359.4	0.0115	3316.5	0.0144	3442.5	0.0218	3442.5	0.0218	0.0129
F7-E-PF9-H-C	3138.9	0.0104	2909.1	0.0121	3057.6	0.0191	3138.9	0.0104	0.0118
F10-N-PF4-H-M[a]	3458.6	0.0098	3350.4	0.0121	3481.0	0.0160	3481.0	0.0160	0.0120
F10-N-PF4-H-C	-	-	-	-	3973.0	0.0192	3973.0	0.0192	0.0149
F10-N-PF9-H-M[a,b]	-	-	-	-	-	-	4371.0	0.0095	0.0072
F10-N-PF9-H-M-R[a,b]	-	-	-	-	-	-	4370.0	0.0105	0.0081
F10-N-PF9-H-C	4183.5	0.0095	3839.8	0.0102	4027.2	0.0194	4183.5	0.0095	0.0146
F10-N-PF9-H-C-R	4105.3	0.0100	3831.7	0.0108	4069.0	0.0190	4105.3	0.0100	0.0139
F10-E-PF4-H-M[a]	-	-	-	-	3229.3	0.0187	3229.3	0.0187	0.0114
F10-E-PF4-H-C	-	-	-	-	3498.9	0.0230	3498.9	0.0230	0.0149
F10-E-PF9-H-M[a]	4185.3	0.0122	3197.4	0.0141	3619.9	0.0199	4185.3	0.0122	0.0109
F10-E-PF9-H-M-R[a]	4164.5	0.0131	3382.5	0.0146	3592.8	0.0189	4164.5	0.0131	0.0115
F10-E-PF9-H-C	4272.1	0.0123	3667.7	0.0152	3859.1	0.0218	4272.1	0.0123	0.0137

Note: F_1 and F_2 as well as the corresponding ε_{c1} and ε_{c2} refer to the axial loads and axial strains of the points before and after the inner pultruded FRP tube failure, respectively. F_c and ε_{cu} refer to the ultimate axial load and ultimate axial strain at outer filament winding FRP tube rupture. F_{max} and $\varepsilon_{c,max}$ are the maximum axial load (which is taken as the larger value between F_1 and F_c) and the corresponding axial strain. $\varepsilon_{h,rup}$ is the hoop rupture strain of the outer filament winding FRP tube. These parameters will be further illustrated in Section 3 of this paper.

[a]Note: The data was firstly tested and reported by Li et al. [21].

[b]Note: The specimens F10-N-PF9-H-M(-R) were not loaded to FRP rupture due to the capacity limit of the machine. Therefore, 0.0072 and 0.0081 refer to the hoop strains corresponding to F_{max} and $\varepsilon_{c,max}$ for the two specimens, instead of the actual hoop rupture strains.

2.2 Material properties

The mixtures of HSC, NC and ECC are presented in Table 2 and are the same as those adopted in Li et al. [21]. It is worth noting that 2% volume polyethylene (PE) fiber was used for the ECC mixture to obtain the ductile tensile strain hardening behavior [37,38]. The PE fibers are with the diameter of 24 μm, length of 12 mm, density of 0.97 g/cm^3, elastic modulus of 120 GPa and tensile strength of 3000 MPa. Material tests including compressive tests on HSC, NC and ECC cylinders and tensile tests on ECC coupons were conducted to obtain the concrete material properties. The test details can be referred to Li et al. [21]. Compressive properties of the HSC, NC and ECC are provided in Table 3. Tensile strength of ECC is 5.0 MPa, with the ultimate tensile strain capacity of 3-4%.

Table 2 Concrete mix proportions (kg/m^3)

Concrete	Water	Cement	Fly ash	Sand	Aggregate	S.P.*	Fiber
HSC	120	603	-	693	1023	10.6	-
NC	165	550	-	624	1062	1.5	-
ECC	310.5	554.4	665.2	443.7	-	13.5	19.4

S.P.*: Super plasticizer.

Table 3 Concrete material properties

Concrete	Compressive cylinder strength (MPa)	Compressive strain	Elastic modulus (GPa)	Poisson's ratio
HSC	95.1	0.0032	36.8	0.21
NC	63.2	0.0026	32.7	0.22
ECC	55.2	0.0046	15.3	0.21

Outer FRP tube in the composite column was manufactured by filament winding process, with the fiber orientation of 80 degree to the longitudinal axis to provide confinement to the inner concrete. By contrast, inner FRP tube in the composite column was manufactured by pultrusion process, with the fiber oriented along the longitudinal axis. Both inner and outer FRP tubes were made of glass fibers and they were of the same batch as those used in Li et al. [21] for the column tests under monotonic loading. Material tests were conducted to obtain the hoop tensile properties (on FRP rings with the height of 50 mm) and axial compressive properties (on FRP rings with the height of 60 mm) for the outer filament winding FRP tubes as well as the axial tensile and compressive properties (on FRP strip coupons) for the inner pultruded FRP tubes. Detailed information of the material test specimens and test methods can be referred to Li et al. [21]. Material properties of the FRP tubes are summarized in Table 4.

Table 4 FRP tube material properties

FRP tube	Thickness (mm)	Tensile properties			Compressive properties		
		Strength (MPa)	Strain	Elastic modulus (GPa)	Strength (MPa)	Strain	Elastic modulus (GPa)
F7	2.5	620.8	0.0156	39.8	70.6	0.0106	9.5

F10	3.5	630.9	0.0164	38.5	84.6	0.0111	9.7
PF4	4.0	185.5	0.0091	20.4	188.7	0.0114	21.8
PF9	9.0	386.3	0.0103	37.5	379.8	0.0116	35.4

Note: Tensile properties refer to the hoop tensile properties for filament winding FRP tubes (F7 and F10) and axial tensile properties for pultruded FRP tubes (PF4 and PF9). Compressive properties refer to axial compressive properties for both filament winding FRP tubes (F7 and F10) and pultruded FRP tubes (PF4 and PF9).

2.3 Test setup and loading

Axial compression tests were conducted on the MTS 815 rock mechanics machine with the load capacity of approximately 4600 kN. Test setup and specimen instrumentation are shown in Fig. 2. Twelve hoop strain gauges with the gauge length of 5 mm and four axial strain gauges with the gauge length of 20 mm were attached in the mid height of the column for strain measurement. Four LVDTs were put between the top and bottom loading plates to monitor the overall axial shortening behavior of the column in the full height region. In order to avoid failure at the ends of the column, three layers of CFRP strips with the width of 20 mm were wrapped around the column near the two ends for strengthening. Capping with high strength gypsum material was adopted to flatten the top and bottom column surfaces and ensure the column was in full contact with the loading plates. Axial loads, strain gauge readings and LVDT readings were recorded by a data logger simultaneously.

Displacement control, with the loading rate of 0.24 mm/min, was adopted for the axial compression tests. Loading scheme for the cyclic compression tests is presented in Fig. 3. The specimen was loaded to the first target unloading displacement, then unloaded to the load level which was approximately 0 kN, followed by the reloading process until reaching the second target unloading displacement that was larger than the first one. The unloading/reloading processes were repeated until the specimen failure. The difference between the target unloading displacements of the two loading cycles next to each other was nearly kept constant. This unloading/reloading procedure was automatically controlled by a pre-set program.

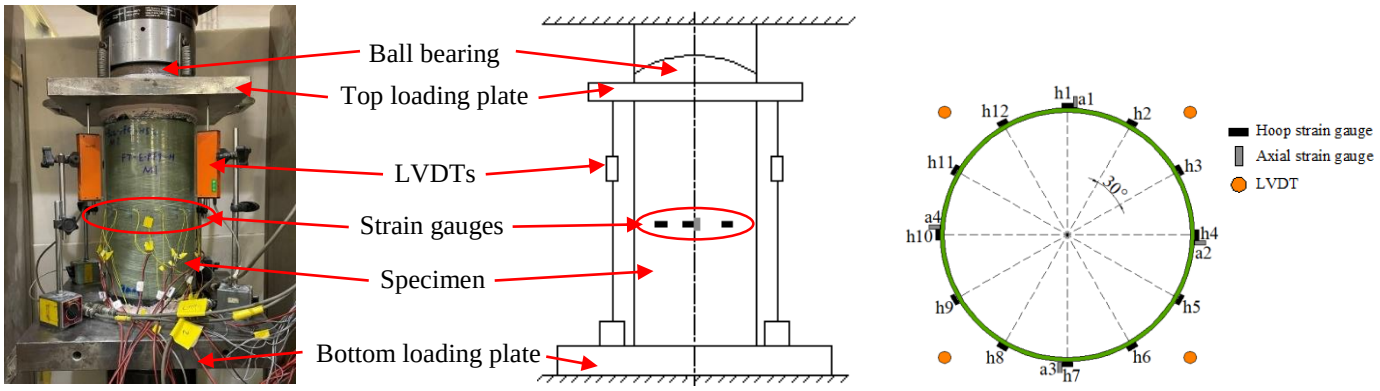

(a) Test setup (b) Specimen instrumentation

Fig. 2 Test setup and specimen instrumentation

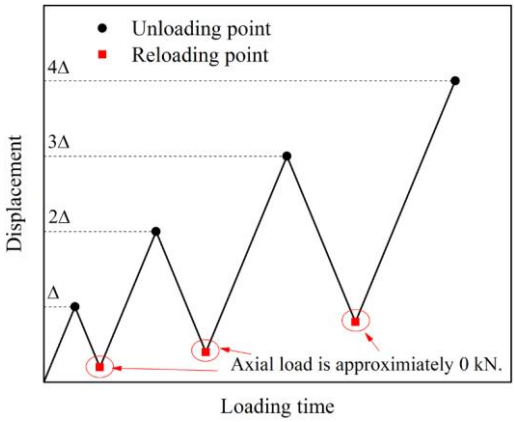

Fig. 3 Loading scheme for cyclic compression

3. Test results and discussions

3.1 Failure modes

Typical failure modes of the tested specimens are shown in Fig. 4. All the specimens failed by outer FRP tube rupture in the hoop direction as shown in Fig. 4(a). White patches can also be noted on the outer FRP tube, indicating the resin failure. The outer FRP tubes were cut and removed after tests to observe the cracking behavior of inner concrete as shown in Fig. 4(b). For FRP-confined HSC columns, large diagonal cracks separated the HSC core from the top to the bottom, indicating the localized and brittle failure. For FRP-concrete double tube composite columns with NC as the ring concrete, the NC would crush at the locations where FRP rupture initiated. When ECC was used as the ring concrete, the columns remained intact with multiple cracks distributed in a relatively uniform manner on the ECC ring surface around the column. When NC ring or ECC ring were further removed, splitting failure of inner pultruded FRP tube could be observed as shown in Fig. 4(c). During the test, tearing sound could be heard before the outer FRP tube rupture, which was corresponding to the inner tube failure. Crushing of the HSC core was also noted as shown in Fig. 4(d). For the tested specimens under monotonic and cyclic compressions, the failure modes are similar as discussed above and no significant differences were observed.

F7-H-M F7-H-C F7-E-PF9-H-M-R F7-E-PF9-H-C F7-N-PF9-H-M F7-N-PF9-H-C

(a) Rupture of outer filament winding FRP tube

F7-H-M F7-H-C F7-E-PF9-H-M-R F7-E-PF9-H-C F7-N-PF9-H-M F7-N-PF9-H-C

(b) Cracking of concrete

(c) Splitting of inner pultruded FRP tube

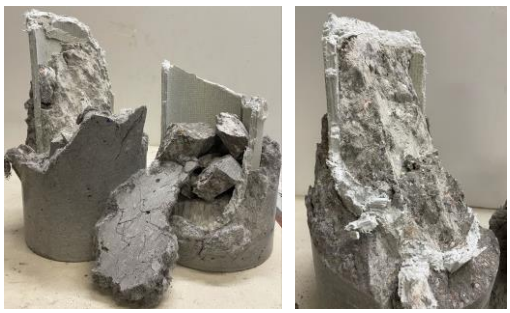

(d) Crushing of HSC core

Fig. 4 Typical failure modes for tested specimens

3.2 Axial load-axial strain responses

Axial load-axial strain curves are presented in Fig. 5 for all the tested specimens. It is worth noting that the axial strains can be obtained through the average readings of the four axial strain gauges as well as calculated based on the average readings of the four LVDTs and the corresponding column heights. During the tests, it was observed that the axial strains determined by the two methods could agree well with each other in the initial elastic stage, while started to deviate from each other when getting into the plastic stage. Due to the non-uniform concrete damage and cracking [39], the differences of the readings from the four axial strain gauges were larger and larger and could no longer reflect the actual axial strain of the column in the plastic stage. Meanwhile, the strain gauges would also be damaged at the later loading stage with relatively large axial deformations. Therefore, the axial strains calculated by the average readings of the LVDTs were adopted in Fig. 5 and the following discussions in this study.

As observed in Fig. 5, the envelope curves of the specimens under cyclic compression were close to the axial load-axial strain curves of the counterpart specimens under monotonic compression. The cyclically loaded specimens could generally exhibit the larger ultimate axial strain than the monotonically loaded specimens, except that the ultimate axial strains for the specimens F7-N-PF4-H-M and F7-N-PF4-H-C were the same as shown in Fig. 5(c). It indicates a larger deformability can be achieved for the composite columns under cyclic loadings, which is also a phenomenon reported in the existing literatures for FRP-confined concrete [28,29].

Axial load-axial strain curves for FRP-confined HSC columns are plotted in Figs. 5(a) and (b). For F7-H specimens as shown in Fig. 5 (a), a significant load drop could be noted after the first peak point. The ultimate loads were lower than the first peak loads, which demonstrated the insufficient confinement provided by the FRP tube. When the outer filament winding FRP tube thickness was increased from F7 to F10 as shown in Fig. 5(b), the ultimate loads were larger than the first peak loads. Axial load-axial strain curves for FRP-concrete double tube composite columns are plotted in Figs. 5(c-j). All the double tube composite columns exhibited the effectively enhanced ultimate load, with much less or no load drops after the first peak compared with the corresponding FRP-confined HSC columns. Meanwhile, the double tube composite columns could develop the obviously improved ultimate axial strains, indicating the better deformability than the counterpart FRP-confined HSC columns. For FRP-concrete double tube composite columns, another load drop was observed in the strain hardening stage at the point

corresponding to the inner pultruded FRP tube failure, which was prior to the outer filament winding FRP tube rupture. Detailed information for the whole process compressive behavior of the double tube composite column under monotonic compression can be referred to Li et al. [21]. For cyclically loaded double tube composite columns, the load drop due to the inner tube failure is less obvious for most of the tested specimens as shown in Figs. 5(c,d,f,h). Specimens F10-N-PF4-C (as shown in Fig. 5(g)) and F10-E-PF4-C (as shown in Fig. 5(i)) did not exhibit this load drop because of the less axial load carried by the inner tube (PF4 as inner tube) and stronger FRP confinement (F10 as outer tube). Key test results of the tested specimens, including the loads before and after the inner tube failure F_1 and F_2 and the corresponding axial strains ε_{c1} and ε_{c2}, the ultimate load and ultimate axial strain F_c and ε_{cu} and the maximum load F_{max} (which is taken as the larger one between F_1 and F_c) and the corresponding axial strain $\varepsilon_{c,max}$, are summarized in Table 1.

Similar to FRP-confined HSC columns, the load carrying capacity of FRP-concrete double tube composite columns would increase with the increase of outer filament winding FRP tube thickness. It can also be noted in Fig. 5 that the load capacity of the double tube composite columns with PF9 as the inner pultruded FRP tube is higher than those with PF4 as the inner pultruded FRP tube. For specimens with ECC as the ring concrete, the load capacity is lower in comparison to the specimens with NC as the ring concrete, which is due to that the compressive strength of ECC is lower than that of NC in this study. Effects of the discussed test variables, including the outer filament winding FRP tube thickness, inner pultruded FRP tube thickness and ring concrete type, on the axial load-axial strain curves are similar for the specimens under monotonic and cyclic loadings.

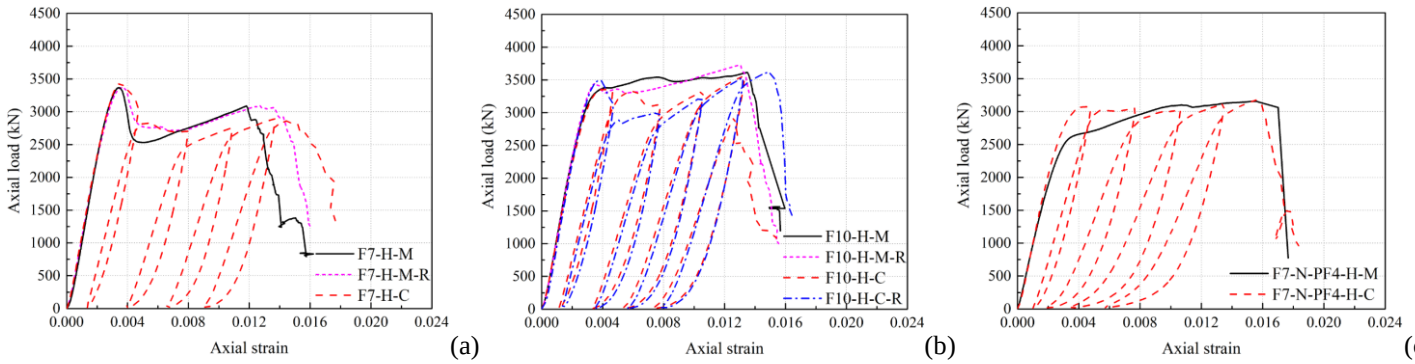

(a) (b) (c)

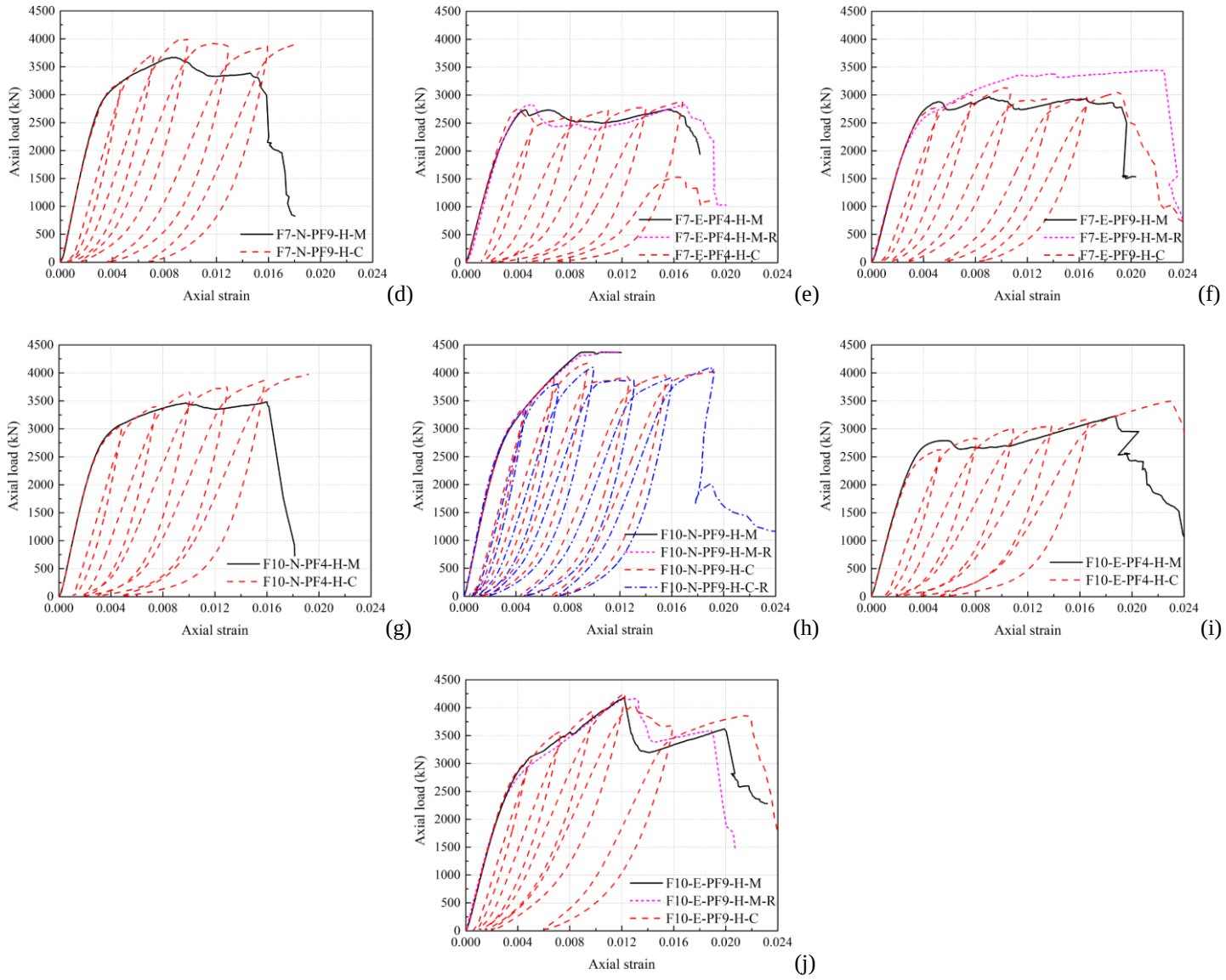

Fig. 5 Axial load-axial strain curves for tested specimens

3.3 Hoop strain-axial strain responses

Hoop strain reflects the lateral dilation of FRP-confined concrete and is closely related to the confining pressure provided by the outer FRP tube. For the tested composite columns, hoop strains can be determined by the average readings of the twelve hoop strain gauges attached on the outer FRP tube surface and plotted versus the corresponding axial strains as shown in Fig. 6. Similar to the axial load-axial strain curves as shown in Fig. 5, the envelope curves of the specimens under cyclic compression were close to the hoop strain-axial strain curves of the counterpart specimens under monotonic compression. This observation is also in agreement with that reported in Chen et al. [36] for FRP-steel dually confined concrete under cyclic axial loading. Larger hoop strains and axial strains at the ultimate point could be noted for the cyclically loaded specimens than those for the monotonically

loaded specimens. Compared with FRP-confined HSC columns, FRP-concrete double tube composite columns exhibited the slower hoop strain development. With the increase of outer filament winding FRP tube thickness, the hoop strain would increase more slowly due to the stronger confinement for both FRP-confined HSC columns and FRP-concrete double tube composite columns. Meanwhile, it could also be noted in Fig. 6 that for the double tube specimens with thicker inner pultruded FRP tube (PF9) or with ECC as the ring concrete, the hoop strain was lower at a given axial strain. It is believed that with the presence of the inner pultruded FRP tube, the HSC core is separated from the concrete ring, so that the concentrated hoop strain on the cracked HSC core cannot be spread out directly. This effect may decrease the overall hoop strain development of the composite column. Meanwhile, it also reflects that ECC ring presents slower lateral dilation behavior. This phenomenon is in line with the observation reported in the literature that the lateral dilation for FRP-confined ECC is lower than that for FRP-confined normal concrete under the same level of confinement due to the presence of fibers in ECC mixture [17,40,41]. The effects of the investigated test variables on the hoop strain-axial strain responses are similar for the specimens under monotonic and cyclic loadings. Average hoop rupture strain $\varepsilon_{h,rup}$ and ultimate axial strain ε_{cu} corresponding to FRP rupture are summarized in Table 1 for the tested specimens.

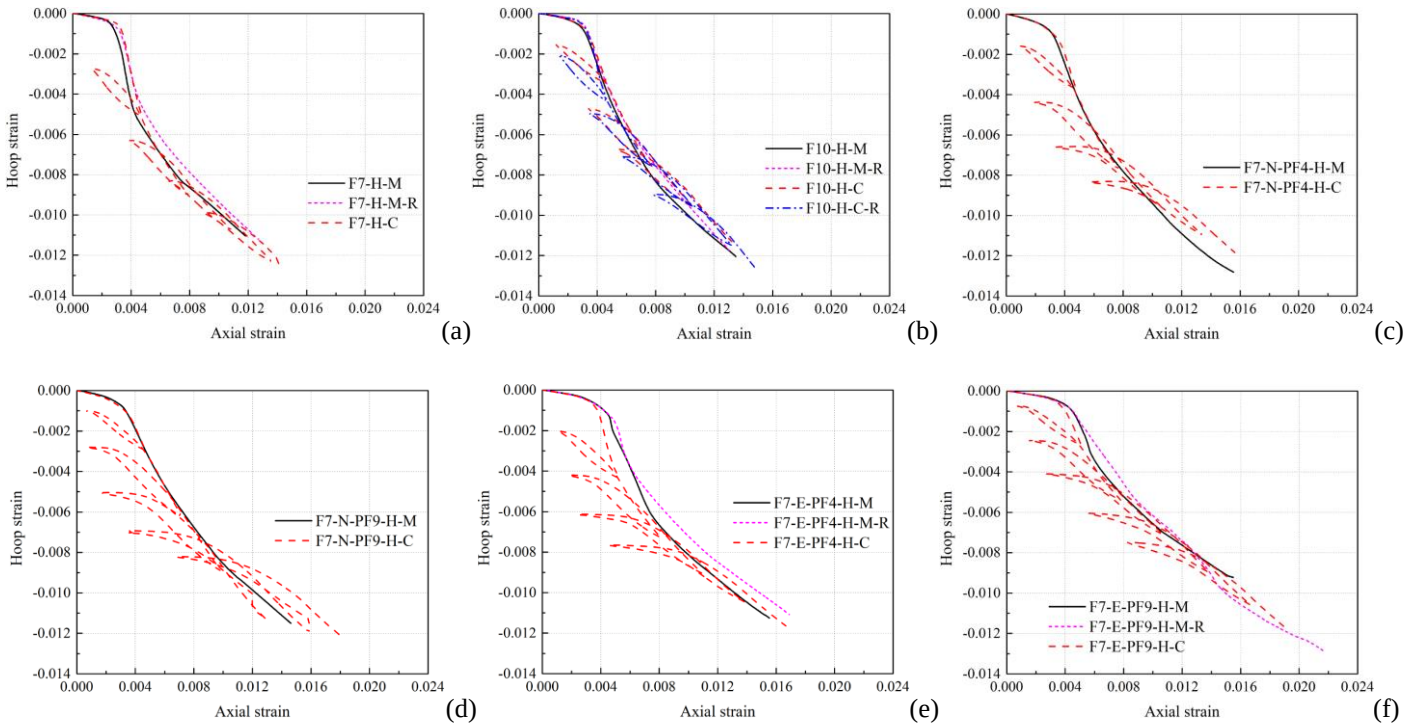

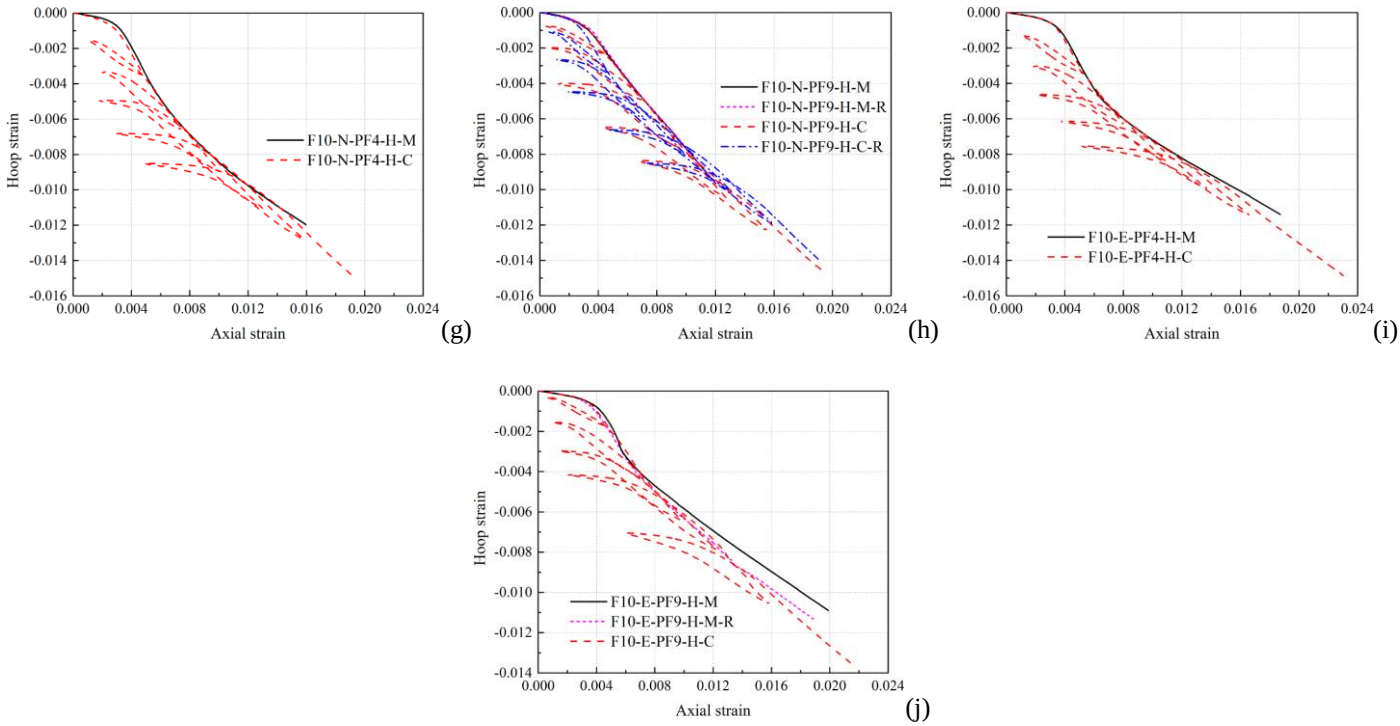

Fig. 6 Hoop strain-axial strain curves for tested specimens

3.4 Hoop strain distributions

With the twelve hoop strain gauges attached on the outer FRP tube surface, the hoop strain distribution behavior can be obtained. Fig. 7 shows the typical hoop strain distributions for the tested columns under monotonic and cyclic loadings. It can be observed that the specimens under cyclic compression could generally develop the relatively more uniform hoop strain distributions in comparison to the counterpart specimens under monotonic compression. This observation agrees with the explanation made by Dang et al. [40] that the cracks in FRP-confined concrete can be more fully developed to result in the more uniform distribution of lateral strain, which consequently leads to the larger ultimate conditions for cyclically loaded specimens, compared with the corresponding monotonically loaded specimens [28]. It is believed that the concrete cracks could be more uniformly distributed during the repeated unloading-reloading cycles, in comparison to that the cracks may tend to be concentrated for monotonically loaded specimens. This more uniform hoop strain could lead to the delayed column failure with improved ultimate axial strain, which is shown in Fig. 7 as well as in Fig. 6 for the hoop strain-axial strain curves.

Compared with the FRP-confined HSC columns as shown in Figs. 7(a) and (b), the hoop strain distribution is more uniform for the FRP-concrete double tube composite columns as shown in Figs. 7(c-j). Li et al. [21] proposed the

failure mechanism for the FRP-concrete double tube composite column under monotonic compression, which related the hoop strain behavior to concrete cracking pattens. It was noted that the inner pultruded FRP tube and the less brittle ring concrete could prevent the concentrated strain from spreading directly from the localized cracked HSC core to the outer filament winding FRP tube, resulting in a more uniform hoop strain distribution. This mechanism is believed to be appliable as well to the composite columns under cyclic compression. Meanwhile, for specimens with ECC as the ring concrete, beneficial effects could also be brought to the hoop strain distribution due to the multiple cracking behavior of ECC which could help to further redistribute the hoop strain and avoid strain concentration [17].

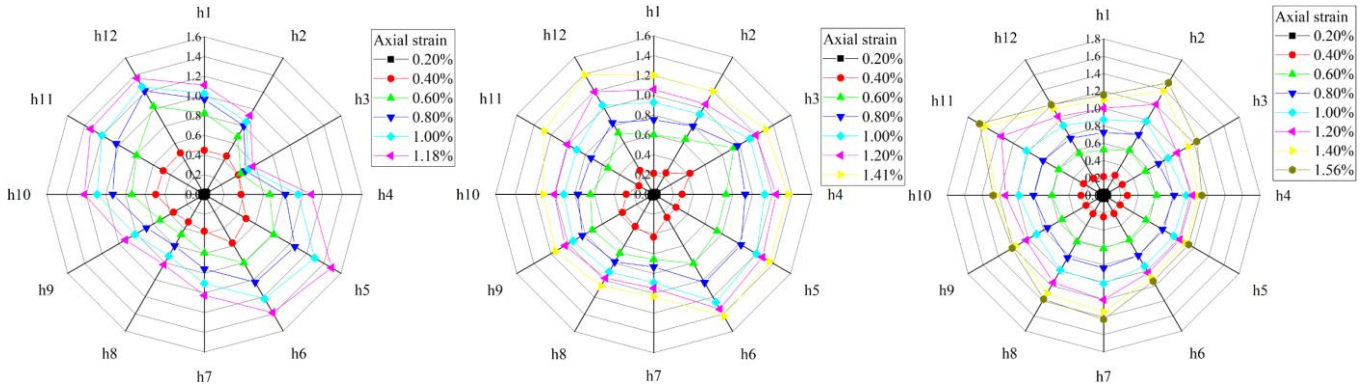

(a) F7-H-M

(b) F7-H-C

(c) F7-N-PF4-H-M

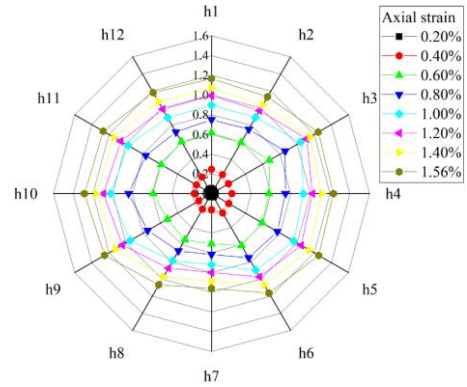

(d) F7-N-PF4-H-C

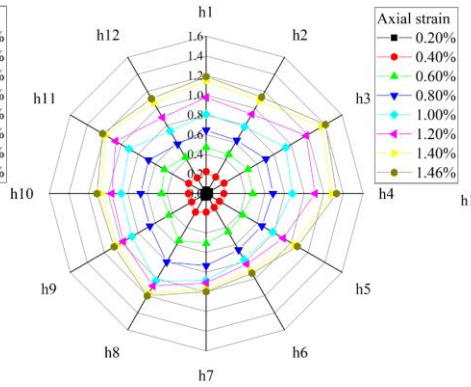

(e) F7-N-PF9-H-M

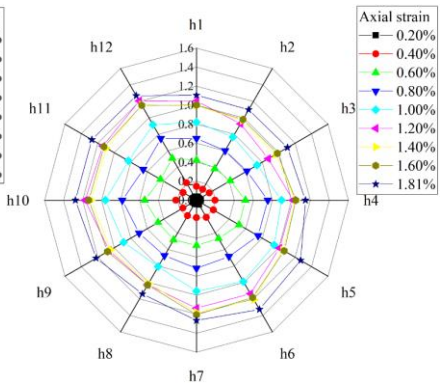

(f) F7-N-PF9-H-C

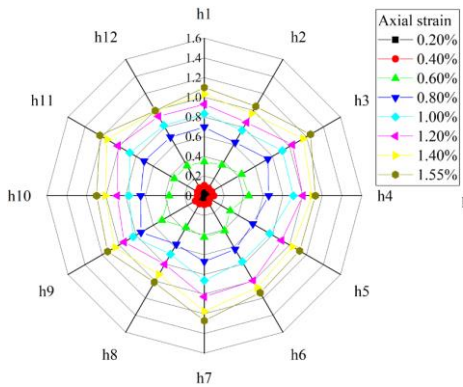

(g) F7-E-PF4-H-M

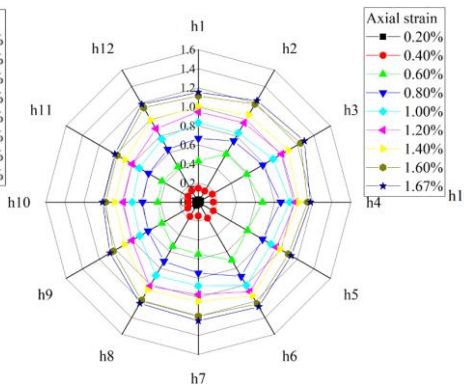

(h) F7-E-PF4-H-C

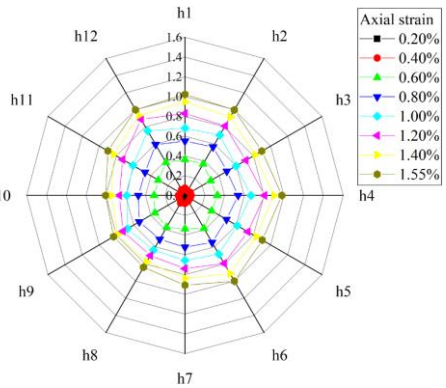

(i) F7-E-PF9-H-M

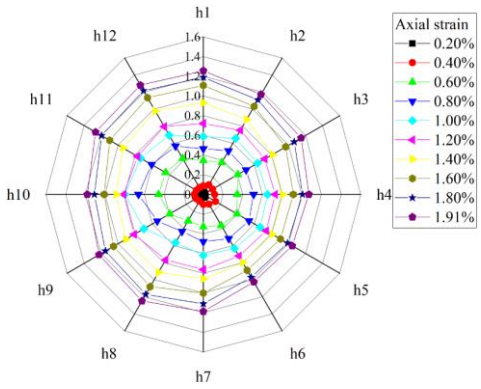

(j) F7-E-PF9-H-C

Fig. 7 Typical hoop strain distributions of the tested specimens

4. Cyclic load-strain model

4.1 Prediction of axial load

In the FRP-concrete double tube composite column, the confinement effect is provided by the outer filament winding FRP tube only. The pultruded FRP tube cannot provide additional confinement to the HSC core, since all the fibers are oriented in the longitudinal direction and the tensile strength in hoop direction is negligible. The design equation for the FRP-concrete double tube composite column under monotonic compression was proposed in Li et al. [21], which can also be used for the composite columns under cyclic compression in this study. It is considered that the total axial load of the composite column can be calculated through the superposition of the axial loads carried by the different components as expressed with the following equation:

$$F = A_{core}\sigma_{core} + A_{ring}\sigma_{ring} + A_F\sigma_F + A_{PF}\sigma_{PF} \quad (1)$$

in which σ_{core} and σ_{ring} are the confined concrete compressive stresses of core concrete and ring concrete; σ_F and σ_{PF} are the axial compressive stresses of outer filament winding FRP tube and inner pultruded FRP tube; A_{core}, A_{ring}, A_{PF} and A_F are the sectional areas of core concrete, ring concrete, inner pultruded FRP tube and outer filament winding FRP tube, respectively. With Eq. (1), the overall axial load-axial strain curve can be generated for the FRP-concrete double tube composite column. The confined compressive stresses of core concrete σ_{core} and ring concrete σ_{ring} can be determined from the corresponding cyclic stress-strain models, which will be discussed in detail in the following sections of this paper.

The compressive stress-strain relations of outer filament winding FRP tubes σ_F can be determined from the ring compression tests [21] and are shown in Fig. 8. Since the outer FRP tube is supported by the inner concrete, its failure can be delayed. It is assumed that the compressive strength is maintained to be unchanged when reaching the ultimate compressive strain till the column failure by outer FRP tube rupture. Meanwhile, the load carried by the FRP tube is quite limited compared with that carried by the inner confined concrete. The assumption has also been widely adopted by the existing literatures for FRP tube confined concrete [11,26,42,43] to simplify the design equations and no significant effect would be caused. Compression tests on the hollow pultruded FRP tubes (with the same height as the composite column) were conducted in Li et al. [21] to obtain its compressive stress-strain behavior. Since the inner tube was embedded between the core concrete and ring concrete, its failure was delayed as well. Meanwhile, the load drop ($F_1 - F_2$ as presented in Table 1) in the strain hardening stage corresponding to the inner pultruded FRP tube failure as shown in Fig. 5 was approximately 30% of the maximum load capacity of the corresponding hollow pultruded FRP tube on average. It indicates that there would be residual capacity contributed by the inner pultruded FRP tube after its failure. To be conservative, 50% of the compressive strength of the corresponding pultruded FRP tubes is considered as the residual strength in the composite columns. The axial strain range corresponding to the inner tube failure is between ε_{c1} and ε_{c2} as presented in Table 1. Therefore, average values of ε_{c1} and ε_{c2} can be calculated respectively based on the obtained test results. The axial stress of inner pultruded FRP tube is unchanged after reaching its compressive strain, then drops from the axial strain ε_{c1} to reach the 50% of the compressive strength at the axial strain ε_{c2}, followed by the unchanged 50% residual strength until column failure by outer FRP tube rupture. The adopted compressive stress-strain relations of PF4 and PF9 are shown in Fig. 8.

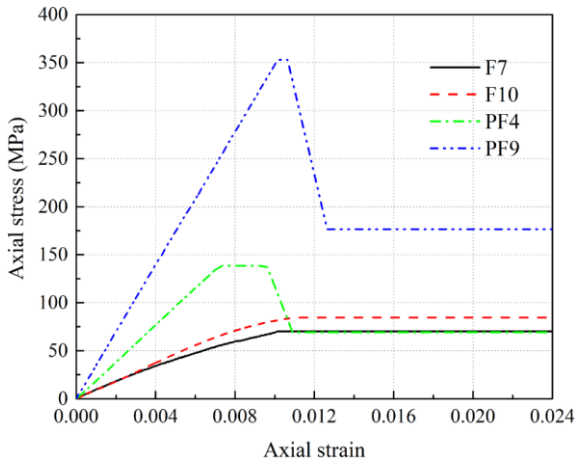

Fig. 8 Compressive stress-strain relations for FRP tubes in the capacity analysis of the composite column

343

344 *4.2 Cyclic stress-strain model and terminology*

345 Typical cyclic stress-strain model for FRP-confined concrete, which consists of the envelope curve, unloading
346 curve and reloading curve, is shown in Fig. 9. The envelope curve is regarded as the upper boundary of the cyclic
347 stress-strain curve. In the unloading path as shown in segment AB in Fig. 9, the stress reduces with the decrease
348 of strain. Axial strain ε_{un} and axial stress σ_{un} at the unloading point A are defined as the unloading strain and
349 unloading stress, respectively. When stress in the unloading curve becomes zero at point B, the corresponding
350 strain is defined as the plastic strain ε_{pl}. Reloading curve starts at point B with the increase of axial stress and
351 strain and intersects with the envelope curve at point D ($\varepsilon_{ret,env}, \sigma_{ret,env}$). At reference point C in the reloading
352 curve, the axial strain ε_{ref} equals to the unloading strain ε_{un}. The corresponding stress σ_{new} at point C is lower
353 than the unloading stress σ_{un} at point A, which reflects the stress deterioration behavior. The cyclic stress-strain
354 models for HSC, NC and ECC under FRP confinement, which are used to generate the load-strain model for the
355 FRP-concrete double tube composite column, are determined by the models of the envelope curve, unloading
356 curve, reloading curve, plastic strain and stress deterioration. These components will be discussed in detail in the
357 following sections of this paper.

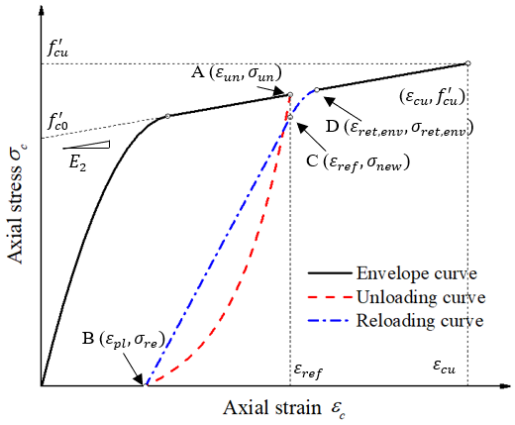

358

359 Fig. 9 Typical stress-strain model for FRP-confined concrete and key parameters

360

361 *4.3 Envelope curves*

362 It is accepted that the envelope curve of FRP-confined concrete under cyclic compression is close to the stress-
363 strain curve of FRP-confined concrete under monotonic compression [28-30]. Lam and Teng [44] proposed the

design-oriented monotonic stress-strain model to predict the compressive behavior of FRP-concrete concrete, which has been widely adopted in the literature [39,42,45,46]. It consists of a parabolic first portion and a linear second portion, with the smooth transition in between. The expressions are shown as follows:

$$\sigma_c = \begin{cases} E_c\varepsilon_c - \frac{(E_c-E_2)^2}{4f'_{c0}}\varepsilon_c^2 & (0 \le \varepsilon_c \le \varepsilon_t) \\ f'_{c0} + E_2\varepsilon_c & (\varepsilon_t < \varepsilon_c \le \varepsilon_{cu}) \end{cases} \quad (2)$$

in which σ_c and ε_c are the axial compressive stress and strain of confined concrete; E_c and f'_{c0} are elastic modulus and compressive strength of unconfined concrete. E_2 is the slope of the linear second portion and can be calculated as follows:

$$E_2 = \frac{f'_{cu}-f'_{c0}}{\varepsilon_{cu}} \quad (3)$$

where f'_{cu} and ε_{cu} are the ultimate compressive strength and ultimate axial strain of FRP-confined concrete. The transition strain ε_t between the parabolic first portion and the linear second portion can be calculated as follows:

$$\varepsilon_t = \frac{2f'_{c0}}{E_c-E_2} \quad (4)$$

Ultimate conditions of f'_{cu} and ε_{cu} are required to be determined to generate the monotonic stress-strain models of FRP-confined HSC, NC and ECC. Lam and Teng [44] and Teng et al. [47] developed the prediction equations of f'_{cu} and ε_{cu} for FRP-confined concrete. They were widely adopted by the subsequent studies [48,49] and design recommendations like United Kingdom Concrete Society [50] and ACI 440.2R-17 [51], with the equation forms expressed as follows:

$$\frac{f'_{cu}}{f'_{c0}} = C_1 + k_1(\rho_K - a)\rho_\varepsilon \quad (5)$$

$$\frac{\varepsilon_{cu}}{\varepsilon_{c0}} = C_2 + k_2 f(\rho_K) g(\rho_\varepsilon) \quad (6)$$

$$\rho_K = \frac{K_l}{f'_{c0}/\varepsilon_{c0}} = \frac{2E_f t_f}{\left(f'_{c0}/\varepsilon_{c0}\right)D} \quad (7)$$

$$\rho_\varepsilon = \frac{\varepsilon_{h,rup}}{\varepsilon_{c0}} \quad (8)$$

in which f'_{c0} and ε_{c0} are compressive strength and strain of unconfined concrete; $\varepsilon_{h,rup}$ is the average FRP hoop rupture strain; E_f and t_f are the elastic modulus and thickness of confining FRP; D is the diameter of confined

concrete; K_l is the confining stiffness; C_1 and C_2 are constants; k_1 and k_2 are strength and strain enhancement coefficients; ρ_K is confinement stiffness ratio and ρ_ε is the strain ratio; a is the confinement stiffness ratio threshold for effective confinement; $f(\rho_K)$ and $g(\rho_\varepsilon)$ are functions of the confinement stiffness ratio and the strain ratio.

Based on the test results presented in the current study, parameters in Eqs. (5) and (6) are calibrated. The following expressions are proposed for the strength predictions:

$$\frac{f'_{cu,HSC}}{f'_{c0,HSC}} = 1 + 3.5(\rho_K - 0.035)\rho_\varepsilon \tag{9}$$

$$\frac{f'_{cu,NC}}{f'_{c0,NC}} = 1 + 3.5(\rho_K - 0.01)\rho_\varepsilon \tag{10}$$

$$\frac{f'_{cu,ECC}}{f'_{c0,ECC}} = 1 + 2.5(\rho_K - 0.01)\rho_\varepsilon \tag{11}$$

where $f'_{cu,HSC}$, $f'_{cu,NC}$ and $f'_{cu,ECC}$ are the compressive strengths of FRP-confined HSC, NC and ECC, while $f'_{c0,HSC}$, $f'_{c0,NC}$ and $f'_{c0,ECC}$ are the unconfined strengths of HSC, NC and ECC. In the equations, $C_1 = 1$ is adopted to keep the unconfined concrete strength unchanged when there is no confinement effect. Strength enhancement coefficient is taken as $k_1 = 3.5$ for FRP-confined normal concrete (both HSC and NC investigated in this study) as suggested by Teng et al. [47] and $k_1 = 2.5$ for FRP-confined ECC as suggested by Dang et al. [40]. Teng et al. [47] suggested $a = 0.01$ based on the test data of FRP-confined concrete with the concrete strength ranging from 33.1 MPa to 47.6 MPa. It is also noted that the effective confinement stiffness ratio could decrease with the increase of concrete strength and brittleness [48]. Therefore, in this study, $a = 0.01$ was adopted for NC and ECC with the relatively low unconfined concrete strength as suggested by Teng et al. [47], while a larger value of a needs to be determined for HSC with higher unconfined compressive strength through the trial-and-error process. It is found that when $a = 0.035$, the predicted results of the total load of the composite column, which was calculated using Eq. (1), can overall best fit the test results. The value of ε_{c0} in ρ_K and ρ_ε is the compressive strain corresponding to the peak strength of unconfined HSC, NC and ECC, which can be obtained from the respective material results. The experimental value of $\varepsilon_{h,rup}$ was used in the calculation. With the proposed Eqs. (9-11) for the ultimate compressive strengths of core concrete and ring concrete, the ultimate load carrying capacity of the tested

specimens can be calculated by Eq. (1) as listed in Table 5. Close agreements between the predicted results and test results can be obtained as presented in Fig. 10(a), with the mean value of 1.01 and Coefficient of Variation (CoV) value of 0.040. It demonstrates the good performance of the proposed Eqs. (9-11) on predicting the ultimate load carrying capacity for the tested composite columns.

Based on Eq. (6), the following equations are proposed for the ultimate axial strain:

$$\frac{\varepsilon_{cu}}{\varepsilon_{c0,lrg}} = 1 + 3.64(\rho_{K,equ})^{0.43}(\rho_{\varepsilon,equ})^{1.02} \tag{12}$$

$$\rho_{K,equ} = \frac{K_l}{f'_{c0,ave}/\varepsilon_{c0,lrg}} = \frac{2E_f t_f}{\left(f'_{c0,ave}/\varepsilon_{c0,lrg}\right)D} \tag{13}$$

$$\rho_{\varepsilon,equ} = \frac{\varepsilon_{h,rup}}{\varepsilon_{c0,lrg}} \tag{14}$$

in which $\rho_{K,equ}$ and $\rho_{\varepsilon,equ}$ are the equivalent confinement stiffness ratio and equivalent strain ratio, respectively. The larger axial strain $\varepsilon_{c0,lrg}$ between core concrete and ring concrete is used to consider the beneficial effect brought to the ultimate axial strain of double tube composite columns to the utmost extent. $f'_{c0,ave}$ is the average unconfined strength of core concrete $f'_{c0,core}$ and ring concrete $f'_{c0,ring}$ and can be calculated as:

$$f'_{c0,ave} = \left(f'_{c0,core}A_{core} + f'_{c0,ring}A_{ring}\right)/(A_{core} + A_{ring}) \tag{15}$$

Prediction results of ultimate axial strain calculated by Eqs. (12-15) are summarised in Table 5 and compered with test results in Fig. 10(b) for the tested specimens. Close agreements with the mean value of 1.01 and CoV value of 0.078 indicate the promising predictions on the ultimate axial strain of the tested composite columns.

With the proposed Eqs. (5-15) for the ultimate conditions, axial stress-strain curves can be generated for FRP-confined HSC, NC and ECC using Eqs. (2-4), followed by the determination of the axial load-axial strain curve for the FRP-concrete double tube composite columns using Eq. (1). Predicted curves for the specimens under monotonic compression are plotted and compared with the corresponding test curves in Fig. 11. Reasonable agreements could be obtained between the predicted results and test results, except that larger deviation is noted for specimen F7-E-PF9-H-M as shown in Fig. 11(e) due to the early failure of inner FRP tube during the test. It indicates that the proposed equations are applicable to predict the overall monotonic compressive behavior of the

FRP-concrete double tube composite columns. Meanwhile, the proposed equations can be used to generate the envelope curve for the composite columns under cyclic compression as well.

Table 5 Design equation predictions on ultimate conditions of tested specimens

Specimen label	Ultimate load carrying capacity			Ultimate axial strain		
	$F_{c,test}$ (kN)	$F_{c,pred}$ (kN)	$F_{c,test}/F_{c,pred}$	$\varepsilon_{cu,test}$	$\varepsilon_{cu,pred}$	$\varepsilon_{cu,test}/\varepsilon_{cu,pred}$
F7-H-M[a]	3086.6	3043.8	1.01	0.0118	0.0127	0.93
F7-H-M-R	3093.7	3042.8	1.02	0.0127	0.0129	0.98
F7-H-C	2863.2	3036.8	0.94	0.0141	0.0140	1.01
F10-H-M	3613.7	3584.1	1.01	0.0135	0.0152	0.89
F10-H-M-R	3729.7	3570.5	1.04	0.0130	0.0148	0.88
F10-H-C	3563.2	3560.4	1.00	0.0133	0.0145	0.92
F10-H-C-R	3625.8	3604.3	1.01	0.0149	0.0158	0.95
F7-N-PF4-H-M	3156.9	3043.5	1.04	0.0156	0.0152	1.03
F7-N-PF4-H-C	3181.8	3009.8	1.06	0.0156	0.0142	1.10
F7-N-PF9-H-M	3385.5	3375.7	1.00	0.0146	0.0140	1.04
F7-N-PF9-H-C	3897.5	3396.1	1.15	0.0181	0.0146	1.24
F7-E-PF4-H-M	2746.3	2814.2	0.98	0.0155	0.0171	0.91
F7-E-PF4-H-M-R	2827.4	2808.6	1.01	0.0169	0.0168	1.00
F7-E-PF4-H-C	2894.8	2825.2	1.02	0.0167	0.0175	0.95
F7-E-PF9-H-M	2925.2	3131.5	0.93	0.0155	0.0148	1.05
F7-E-PF9-H-M-R	3442.5	3234.7	1.06	0.0218	0.0190	1.15
F7-E-PF9-H-C	3057.6	3205.6	0.95	0.0191	0.0177	1.08
F10-N-PF4-H-M	3481.0	3531.3	0.99	0.0160	0.0160	1.00
F10-N-PF4-H-C	3973.0	3734.7	1.06	0.0192	0.0191	1.00
F10-N-PF9-H-M*	4371.0	4253.7	1.03	-	-	-
F10-N-PF9-H-M-R*	4370.0	4314.7	1.01	-	-	-
F10-N-PF9-H-C	4027.2	4051.9	0.99	0.0194	0.0189	1.03
F10-N-PF9-H-C-R	4069.0	4004.4	1.02	0.0190	0.0181	1.05
F10-E-PF4-H-M	3229.3	3254.5	0.99	0.0187	0.0189	0.99
F10-E-PF4-H-C	3498.9	3461.7	1.01	0.0230	0.0234	0.98
F10-E-PF9-H-M	3619.9	3571.8	1.01	0.0199	0.0184	1.08
F10-E-PF9-H-M-R	3592.8	3605.9	1.00	0.0189	0.0192	0.99
F10-E-PF9-H-C	3859.1	3731.0	1.03	0.0218	0.0220	0.99
Mean			1.01			1.01
CoV			0.040			0.078

*Note: For specimens F10-N-PF9-H-M(R), the ultimate load carrying capacity is referring to the maximum axial load recorded in tests.

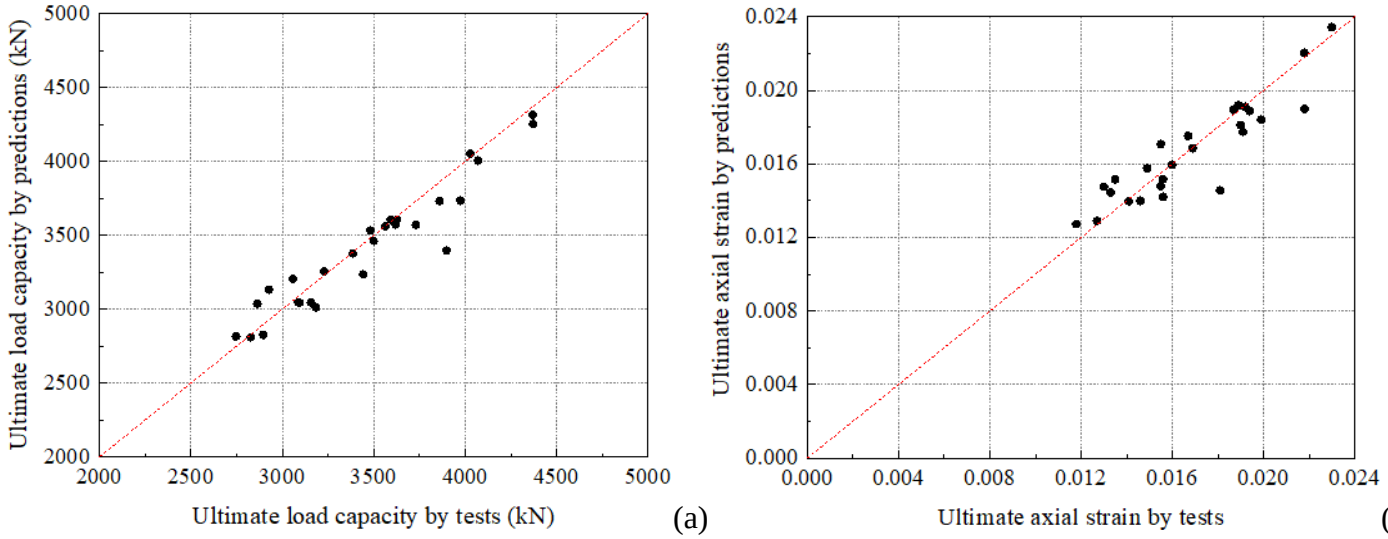

Fig. 10 Comparisons between predicted results and test results for the ultimate conditions of the tested composite columns

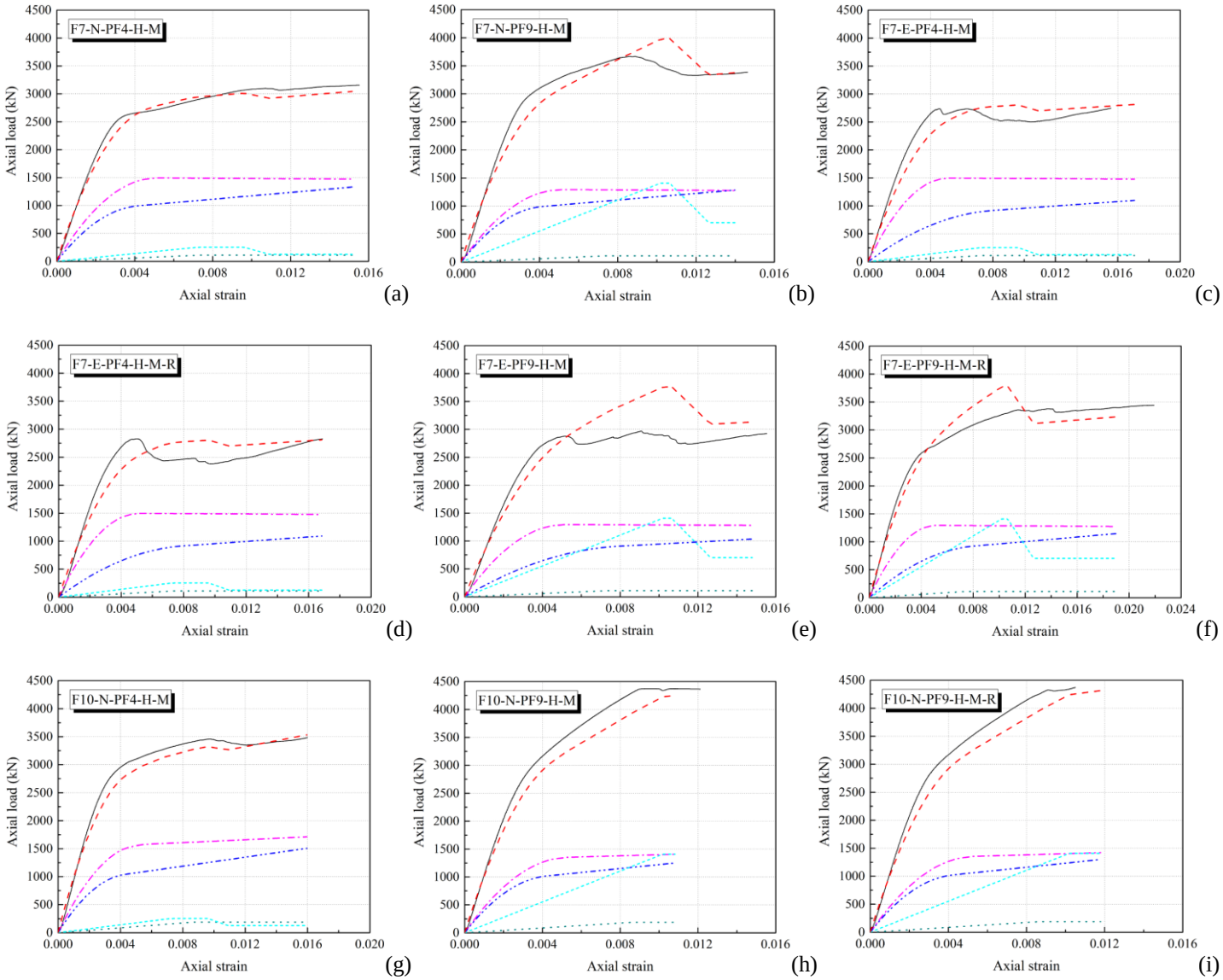

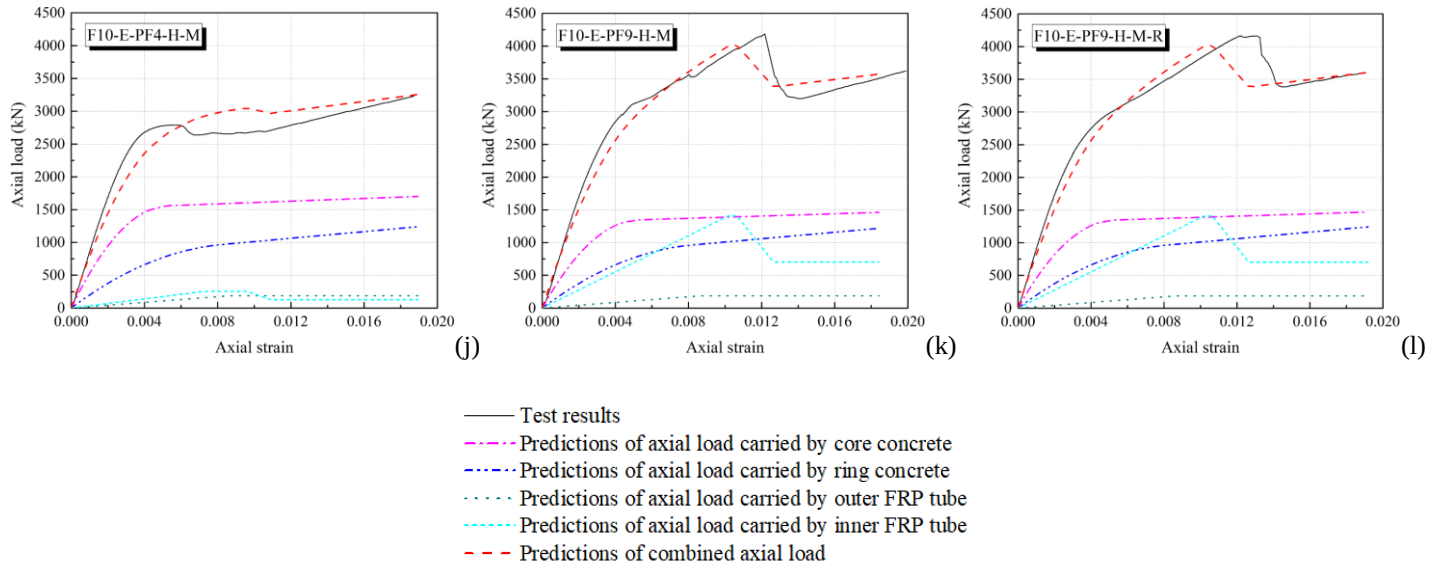

Fig. 11 Predictions of monotonic axial load-axial strain curves for FRP-concrete double tube composite columns

4.4 Unloading curves

Typical unloading curve of FRP-confined concrete is shown in Fig. 9, in which the axial stress will decrease to zero when the axial strain decreases to plastic strain. For FRP-concrete double tube composite columns, however, the axial strain is much smaller corresponding to the point at which the load is zero as shown in Fig. 5. It indicates that the unloading behavior of FRP-concrete double tube composite column is different from that of the normal FRP-confined concrete column. In Fig. 12, it shows the typical unloading load-strain curve for the double tube composite column. At the stage of low axial load level in the unloading curve, the axial load nearly decreases linearly with the decrease of the axial strain. In previous literatures on FRP-concrete-steel double skin tubular columns (DSTCs) under cyclic axial compression [11,52], it is reported that the stress in steel tube will reach zero first before the axial load of the composite column reduces to zero in the unloading process, because of the larger plastic strain component of steel than that of the concrete [52]. Similarly, with the linear behavior of pultruded FRP and the plastic behavior of concrete, the plastic strain component of the inner pultruded FRP tube is smaller than that of the concrete in the FRP-concrete double tube composite column. Inner pultruded FRP tube and core concrete / ring concrete will not reach to the zero stress simultaneously in the unloading process. The axial stress in core concrete and ring concrete will become zero when reaching certain axial strain, which is termed as the plastic strain of confined concrete. At the same strain, the pultruded FRP tube is not unloaded completely. With further unloading, the stress in pultruded FRP tube will continue to decrease, while the core concrete and ring

concrete may remain the zero stress or even develop tensile stress. For simplification, it is assumed that for the core concrete and ring concrete, the zero stress will be remained unchanged after reaching the strain $\varepsilon_{pl,1}$, which is plastic strain of the confined concrete. For outer filament winding FRP tube and inner pultruded FRP tube, the stress will decrease linearly from the unloading strain to the strain $\varepsilon_{pl,2}$, which can be regarded as the plastic strain of the whole FRP-concrete double tube composite column. When reaching the strain $\varepsilon_{pl,2}$, the stresses in both concrete and FRP tubes are zero, so that the total axial load of the composite column is zero as well. For $\varepsilon_{pl,2}$, it is easy to obtain for each loading cycle based on the test results. Tangent slope was calculated in the unloading curve. It is found that the tangent slope $E_{un,1}$ between the point P to the point with plastic strain $\varepsilon_{pl,2}$ is nearly a constant. The axial load could present some fluctuations when it is close to zero, so that ±10% margins are allowed for $E_{un,1}$. Therefore, the point P in the ending part of the unloading curve is determined in the way that between point P and the point with plastic strain $\varepsilon_{pl,2}$, the tangent slope of the load-strain curve is a constant of $E_{un,1}$ with ±10% margins; while before the point P, the tangent slope increases quickly and is much larger than $E_{un,1}$ (when looking backwards in the unloading curve from point P to the unloading point). For the point P, it is corresponding to the plastic strain $\varepsilon_{pl,1}$. With this approach, plastic strain $\varepsilon_{pl,1}$ for each unloading curve can be obtained. Detailed discussions on the plastic strains $\varepsilon_{pl,1}$ and $\varepsilon_{pl,2}$ will be presented in Section 4.5 of this paper.

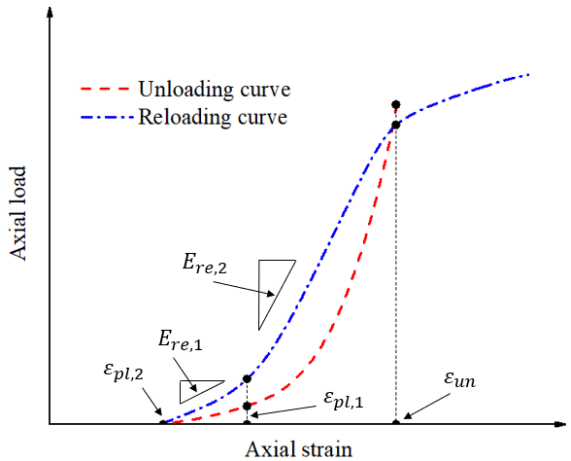

Fig. 12 Typical unloading and reloading curves for FRP-concrete double tube composite column

In Table 6, it summarizes five existing unloading models that have been proposed and adopted for FRP-confined concrete with various concrete strengths and confinement levels [29-33]. These unloading models are used to calculate the unloading stress-strain curves for FRP-confined HSC, NC and ECC, respectively. Axial load-axial

485 strain curves for the cyclically loaded FRP-concrete double tube composite columns can then be determined with
486 Eq. (1) and evaluated through comparing with test results as shown in Fig. 13. As mentioned above, the axial load
487 carried by the FRP tubes is considered to decrease linearly in the unloading process. It is observed that unloading
488 curves predicted by the five existing models are generally in good agreements with each other and can match well
489 with the test curves, except that larger deviations of Yu et al.'s model [30] can be noted at larger axial strains. It
490 indicates that these existing models can be used to predict the unloading behavior of the FRP-concrete double tube
491 composite columns.

492 It is worth noting that the actual unloading strains ε_{un} and plastic strains $\varepsilon_{pl,1}$ and $\varepsilon_{pl,2}$ were used in the calculation,
493 so that the accuracy of predicted curves is only related to the unloading model. Unloading stresses of core concrete
494 and ring concrete cannot be determined directly in the composite column. They were firstly calculated based on
495 the corresponding envelope model as presented in Section 4.3 of this paper with the corresponding unloading
496 strains, followed by the determination of the unloading load of the composite column with Eq. (1). The unloading
497 load of the predicted curves was also kept the same as that of the test curve to ensure that it would not influence
498 the comparison of the unloading model. Therefore, the same increment factor or reduction factor, which depends
499 on the predicted value being lower or higher than the test value, was adopted for core concrete and ring concrete
500 to calculate the new unloading stresses that could ensure the unloading load of the predicted value being the same
501 as that of the test value for the unloading model calculation in Fig. 13.

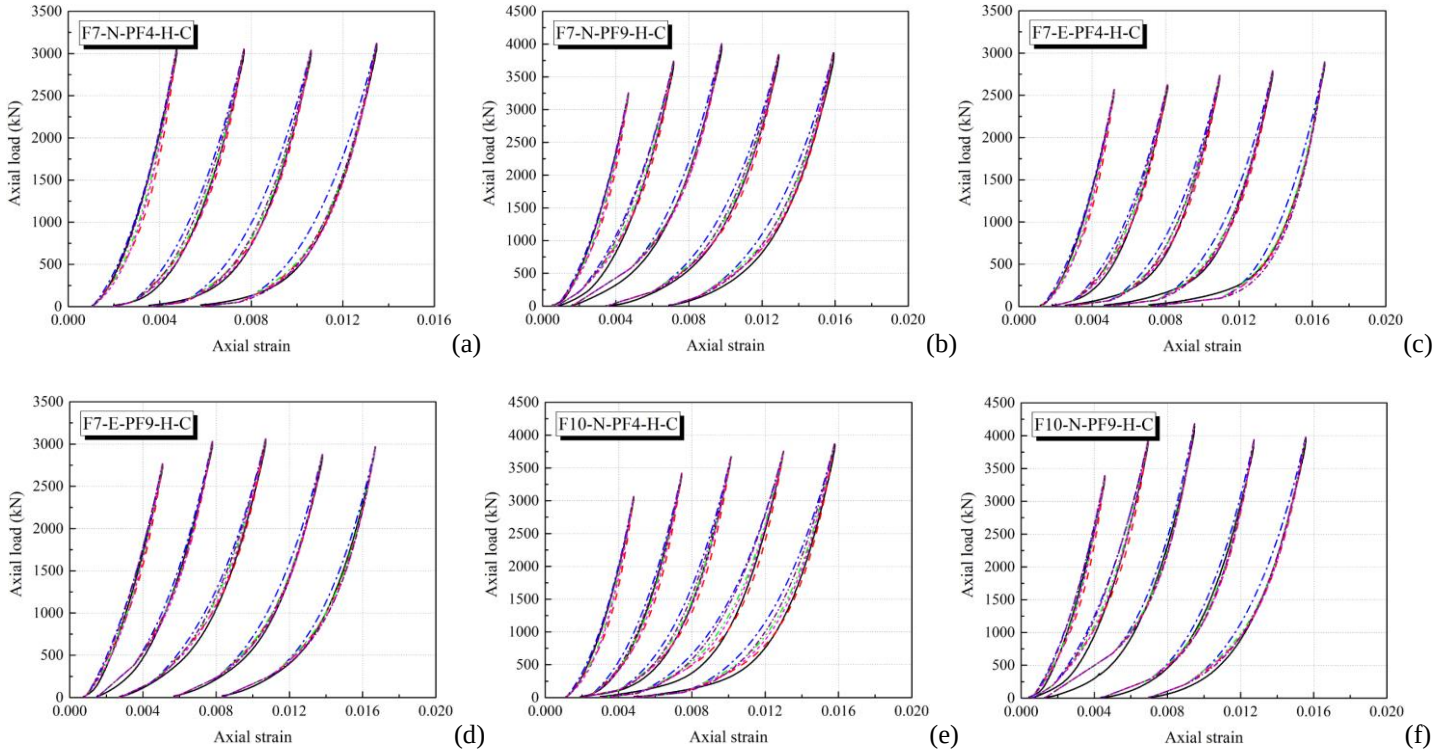

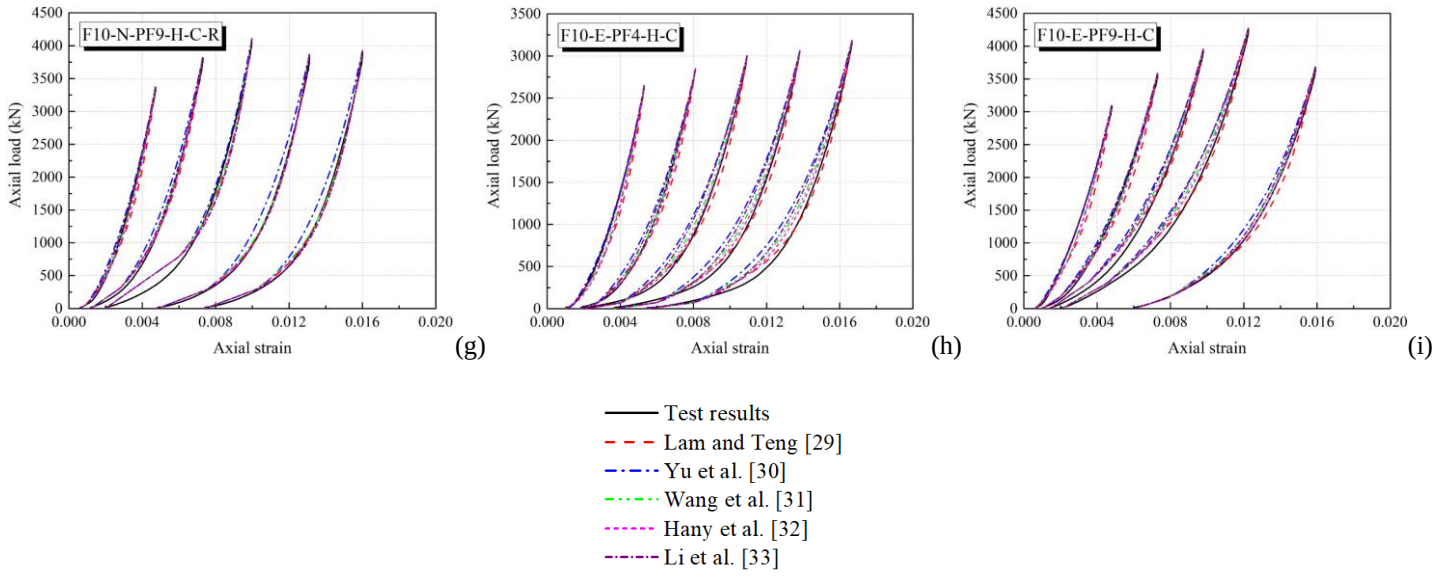

Fig. 13 Comparisons of unloading path between test results and predictions by existing unloading models

507

Table 6 Existing cyclic stress-strain models for FRP-confined concrete

Component	Lam and Teng [29]	Yu et al. [30]	Wang et al. [31]	Hany et al. [32]	Li et al. [33]
Unloading model	$\sigma_c = a\varepsilon_c^{\eta} + b\varepsilon_c + c$ $a = \frac{\sigma_{un} - E_{un,0}(\varepsilon_{un} - \varepsilon_{pl})}{\varepsilon_{un}^{\eta} - \varepsilon_{pl}^{\eta} - \eta\varepsilon_{pl}^{\eta-1}(\varepsilon_{un} - \varepsilon_{pl})}$ $b = E_{un,0} - \eta\varepsilon_{pl}^{\eta-1}a$ $c = -a\varepsilon_{pl}^{\eta} - b\varepsilon_{pl}$ $E_{un,0} = \min(\frac{0.5f'_{c0}}{\varepsilon_{un}}, \frac{\sigma_{un}}{\varepsilon_{un} - \varepsilon_{pl}})$ $\eta = 350\varepsilon_{un} + 3$	Same as Lam and Teng [29] except for η $\eta = 40(350\varepsilon_{un} + 3)/f'_{c0}$	$\frac{\sigma_c}{\sigma_{un}} = B_0(\frac{\varepsilon_c - \varepsilon_{pl}}{\varepsilon_{un} - \varepsilon_{pl}})^{B_1} + (1 - B_0)(\frac{\varepsilon_c - \varepsilon_{pl}}{\varepsilon_{un} - \varepsilon_{pl}})$ $B_0 = 0.5 + 0.3(\frac{f_l}{f'_{c0}})^{0.07} - 0.1(\frac{f_{ls}}{f'_{c0}})^{0.04}$ For $\varepsilon_{un} \le 0.02$, $B_1 = -0.02\left(\frac{\varepsilon_{un}}{\varepsilon_{c0}}\right)^2 + 0.46\left(\frac{\varepsilon_{un}}{\varepsilon_{c0}}\right) + 1.76$ For $\varepsilon_{un} > 0.02$, $B_1 = 4.36$	$\frac{\sigma_c}{\sigma_{un}} = B_0(\frac{\varepsilon_c - \varepsilon_{pl}}{\varepsilon_{un} - \varepsilon_{pl}})^{B_1} + (1 - B_0)(\frac{\varepsilon_c - \varepsilon_{pl}}{\varepsilon_{un} - \varepsilon_{pl}})$ $B_0 = 0.8$ $B_1 = 2.172\left(\frac{\varepsilon_{un}}{\varepsilon_{c0}}\right)^{0.324}$	$\sigma_c = E_{un,0}\left(\frac{\varepsilon_c}{\varepsilon_{pl}}\right)^m(\varepsilon_c - \varepsilon_{pl})$ $\frac{E_{un,0}}{E_c} = 0.21(\frac{f'_{c0}}{f'_{30}})^{0.195}\rho^{-0.031}(\frac{\varepsilon_{un}}{\varepsilon_{c0}})^{-1.115}$ $m = \log_{(\frac{\varepsilon_{un}}{\varepsilon_{pl}})}(\frac{\sigma_{un}}{E_{un,0}(\varepsilon_{un} - \varepsilon_{pl})})$
Plastic strain	For $0 < \varepsilon_{un} \le 0.001$, $\varepsilon_{pl} = 0$ For $0.001 < \varepsilon_{un} < 0.0035$, $\varepsilon_{pl} = [1.4(0.87 - 0.004f'_{c0}) - 0.64](\varepsilon_{un} - 0.001)$ For $0.0035 \le \varepsilon_{un} \le \varepsilon_{cu}$, $\varepsilon_{pl} = (0.87 - 0.004f'_{c0})\varepsilon_{un} - 0.0016$	For $0 < \varepsilon_{un} \le 0.001$, $\varepsilon_{pl} = 0$ For $0.001 < \varepsilon_{un} \le 0.0035$, $\varepsilon_{pl} = 0.184\varepsilon_{un} - 0.0002$ For $0.0035 < \varepsilon_{un} \le \varepsilon_{cu}$, $\varepsilon_{pl} = 0.703\varepsilon_{un} - 0.002$	For $0 < \varepsilon_{un} \le 0.001$, $\varepsilon_{pl} = 0$ For $0.001 < \varepsilon_{un} \le 0.004$, $\varepsilon_{pl} = 0.42\varepsilon_{un} - 0.0004$ For $0.004 < \varepsilon_{un} \le \varepsilon_{cu}$, $\varepsilon_{pl} = 0.815\varepsilon_{un} - 0.002$	For $0 < \varepsilon_{un} \le 0.001$, $\varepsilon_{pl} = 0$ For $0.001 < \varepsilon_{un} \le 0.0035$, $\varepsilon_{pl} = 0.4552\varepsilon_{un} - 0.0003$ For $0.0035 < \varepsilon_{un} \le \varepsilon_{cu}$, $\varepsilon_{pl} = 0.7827\varepsilon_{un} - 0.0014$	For $0 < \varepsilon_{un} \le 0.001$, $\varepsilon_{pl} = 0$ For $0.001 < \varepsilon_{un} \le \varepsilon_{cu}$, $\varepsilon_{pl} = 0.353\left(\frac{f'_{c0}}{f'_{30}}\right)^{-0.4}(\varepsilon_{un} - 0.001) + 3.36\rho^{-0.178}(\varepsilon_{un} - 0.001)^{1.414}$
Stress deterioration	For $0 < \varepsilon_{un} \le 0.001$, $\varphi = 1$ For $0.001 < \varepsilon_{un} < 0.002$, $\varphi = 1 - 80(\varepsilon_{un} - 0.001)$ For $0.002 \le \varepsilon_{un} \le \varepsilon_{cu}$, $\varphi = 0.92$	For $0 < \varepsilon_{un} \le 0.001$, $\varphi = 1$ For $0.001 < \varepsilon_{un} \le 0.0035$, $\varphi = 1 - 32(\varepsilon_{un} - 0.001)$ For $0.0035 < \varepsilon_{un} \le \varepsilon_{cu}$, $\varphi = 0.92$	$\varphi = 0.912$	For $0 < \varepsilon_{un} \le 0.001$, $\varphi = 1$ For $0.001 < \varepsilon_{un} \le \varepsilon_{cu}$, $\varphi = 0.938$	N.A.
Reloading model	For $\varepsilon_{re} \le \varepsilon_c \le \varepsilon_{ref}$, $\sigma_c = \sigma_{re} + E_{re}(\varepsilon_c - \varepsilon_{re})$ For $\varepsilon_{ref} \le \varepsilon_c \le \varepsilon_{ret,env}$, $\sigma_c = A\varepsilon_c{}^2 + B\varepsilon_c + C$ $E_{re} = (\sigma_{new} - \sigma_{re})/(\varepsilon_{ref} - \varepsilon_{re})$ $\sigma_{new} = \varphi\sigma_{un}$ $B = E_{re} - 2A\varepsilon_{ref}$ $C = \sigma_{new} - A\varepsilon_{ref}{}^2 - B\varepsilon_{ref}$ For $\varepsilon_{ret,env} < \varepsilon_t$, $A = \frac{(E_C - E_2)^2(E_{re}\varepsilon_{ref} - \sigma_{new}) + (E_C - E_{re})^2 f'_{c0}}{4(\sigma_{new} - E_c\varepsilon_{ref})f'_{c0} + (E_C - E_2)^2\varepsilon_{ref}{}^2}$ $\varepsilon_{ret,env} = \frac{E_c - B}{2A + \frac{(E_C - E_2)^2}{f'_{c0}}}$ For $\varepsilon_{ret,env} \ge \varepsilon_t$, $A = \frac{(E_{re} - E_2)^2}{4(\sigma_{new} - f'_{c0} - E_2\varepsilon_{ref})}$ $\varepsilon_{ret,env} = \frac{E_2 - B}{2A}$	Same as Lam and Teng [29]	$\sigma_c = E_{re}(\varepsilon_c - \varepsilon_{pl})$ $E_{re} = \frac{\sigma_{new}}{\varepsilon_{un} - \varepsilon_{pl}}$ $\sigma_{new} = \varphi\sigma_{un}$	$\sigma_c = E_{re}(\varepsilon_c - \varepsilon_{pl})$ $E_{re} = \frac{\sigma_{new}}{\varepsilon_{un} - \varepsilon_{pl}}$ $\sigma_{new} = \varphi\sigma_{un}$	$\sigma_c = \frac{(E_{re} - E_2)(\varepsilon_c - \varepsilon_{pl})}{(1 + (\frac{(E_{re} - E_2)(\varepsilon_c - \varepsilon_{pl})}{f_r})^n)^{1/n}} + E_2(\varepsilon_c - \varepsilon_{pl})$ $\frac{E_{re}}{E_c} = (\frac{f'_{c0}}{f'_{30}})^{0.032}\bar{\varepsilon}^{-0.409} - 0.317\rho^{-0.064\bar{\varepsilon}}$ For $E_2 \ge 0$, $\frac{f_r}{f'_{c0}} = 0.693\frac{\sigma_{un}}{f'_{c0}} + 0.337\rho^{-0.053}$ For $E_2 < 0$, $\frac{f_r}{f'_{c0}} = 0.969\frac{\sigma_{un}}{f'_{c0}} + 1.981\rho^{-2.012}$ $\bar{\varepsilon} = \varepsilon_{un}/\varepsilon_{c0} \le 10$ $n = 2.61\left(\frac{\varepsilon_{un}}{\varepsilon_{c0}}\right) + 4.88$

508

4.5 Plastic strains

As discussed in Section 4.4 of this paper, $\varepsilon_{pl,1}$ can be regarded as the plastic strain of confined concrete and $\varepsilon_{pl,2}$ can be regarded as the plastic strain of the FRP-concrete double tube composite column. $\varepsilon_{pl,1}$ and $\varepsilon_{pl,2}$ are collected from each unloading curve of the tested specimens and plotted against the corresponding unloading strains ε_{un} in Fig. 14. It can be observed that the plastic strain $\varepsilon_{pl,1}$ for confined concrete is basically following the linear trend with unloading strain, which is in line with the existing plastic strain models [29-33] for FRP-confined concrete as presented Table 6. For plastic strain $\varepsilon_{pl,2}$, however, obvious non-linear relation with unloading strain can be noted, which is due to the extended unloading process of the FRP tubes after the complete unloading of concrete.

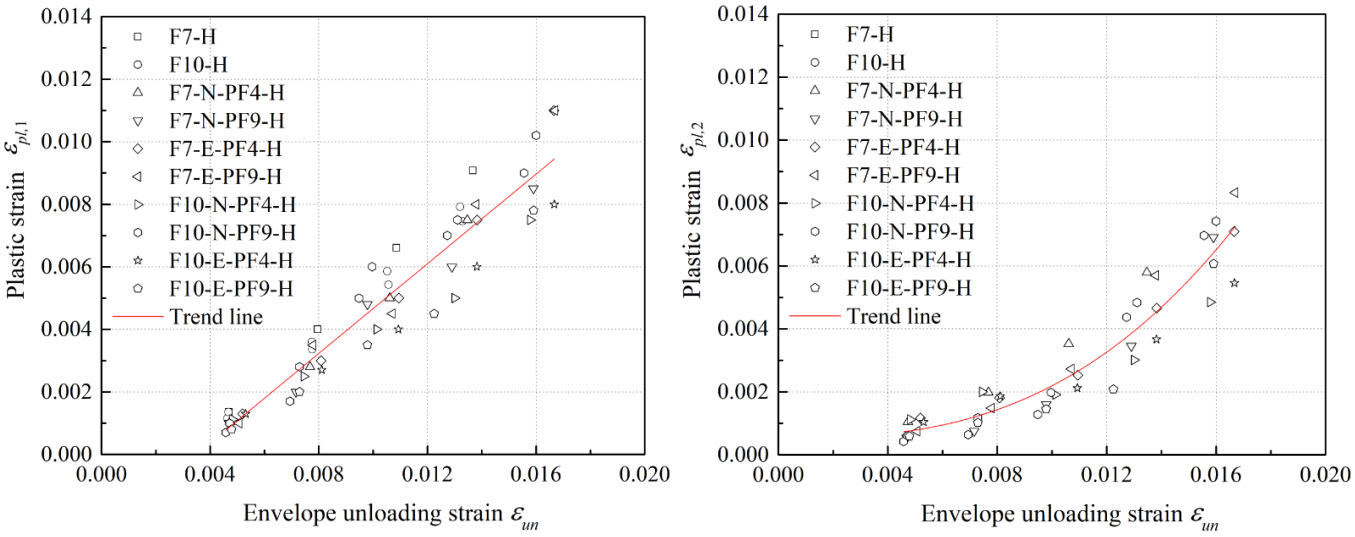

(a) Plastic strain $\varepsilon_{pl,1}$ (b) Plastic strain $\varepsilon_{pl,2}$

Fig. 14 Plastic strains at different unloading strains for the tested specimens

Prediction equations for plastic strains $\varepsilon_{pl,1}$ and $\varepsilon_{pl,2}$ are proposed based on the obtained test results as follows:

$$\varepsilon_{pl,1} = 0.717\varepsilon_{un} - 0.0025 \quad (16)$$

$$\varepsilon_{pl,2} = 481.12(\varepsilon_{un})^{2.732} - 0.0005363 \quad (17)$$

in which linear function is adopted for $\varepsilon_{pl,1}$ and power function is adopted for $\varepsilon_{pl,2}$. Comparisons between the predicted results and test results of the plastic strains $\varepsilon_{pl,1}$ and $\varepsilon_{pl,2}$ are presented in Figs. 15 and 16, respectively. Predictions of $\varepsilon_{pl,1}$ calculated by the existing plastic models listed in Table 6 are also shown in Fig. 15 for

comparison. The close agreements between the predicted results by the proposed models and the test results indicate that the proposed equations could provide reasonable predictions on the plastic strain behavior for the FRP-concrete double tube composite columns under cyclic compression. It is noted that Eqs. (16) and (17) are proposed with the obtained test data in the current study. The applicability may need to be further examined with larger database in future studies.

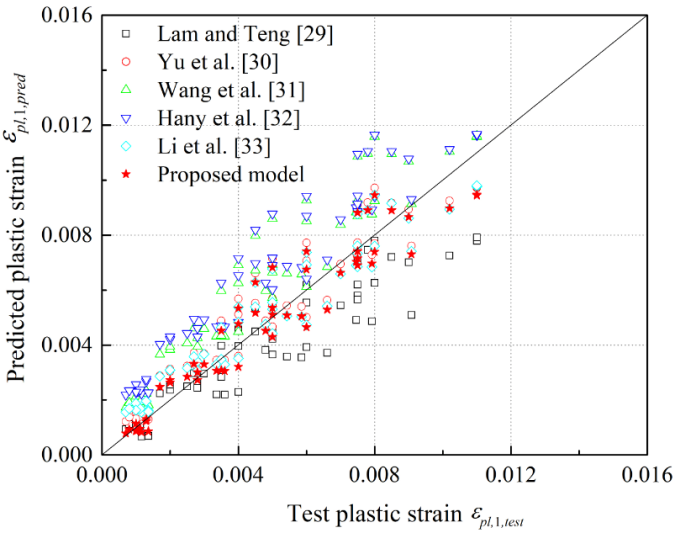

$\varepsilon_{pl,1,test}/\varepsilon_{pl,1,pred}$:

Models	Mean	CoV
Lam and Teng [29]	1.21	0.266
Yu et al. [30]	0.89	0.189
Wang et al. [31]	0.72	0.214
Hany et al. [32]	0.67	0.256
Li et al. [33]	0.89	0.232
Proposed model	1.02	0.193

Fig. 15 Comparisons between predicted results and test results of plastic strain $\varepsilon_{pl,1}$

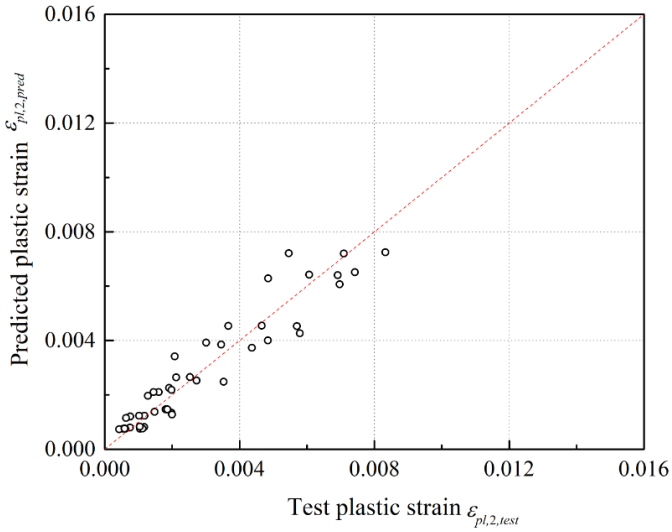

Fig. 16 Comparisons between predicted results and test results of plastic strain $\varepsilon_{pl,2}$

4.6 Stress deterioration

As shown in Fig. 9, the axial stress in the reloading curve σ_{new} is lower that the axial stress in the unloading curve σ_{un} at the same unloading strain ε_{un}. Stress deterioration φ, which is defined as follows, is used to reflect the damage behavior of concrete under cyclic loading:

$$\varphi = \frac{\sigma_{new}}{\sigma_{un}} \tag{18}$$

It Table 6, it summarizes the value of φ is in the range of 0.912 to 0.938 as proposed by the existing models. In the FRP-concrete double tube composite column, the stress deteriorations for core concrete and ring concrete are considered to be same. Therefore, stress deterioration for each loading cycle can be calculated based on the ratio of the axial load carried by the core concrete and ring concrete at the unloading strain ε_{un} in the reloading curve to that at the unloading strain ε_{un} in the unloading curve. The axial load carried by the core concrete and ring concrete can be determined by subtracting the axial load carried by the inner and outer FRP tubes from the total axial load carried by the composite column. In Fig. 17, it shows that the stress deterioration is generally irrelevant to ring concrete material, confinement level and unloading strain. $\varphi = 0.915$ is adopted as the stress deterioration for the core concrete and ring concrete in the FRP-concrete double tube composite column, based on the mean value of the test data.

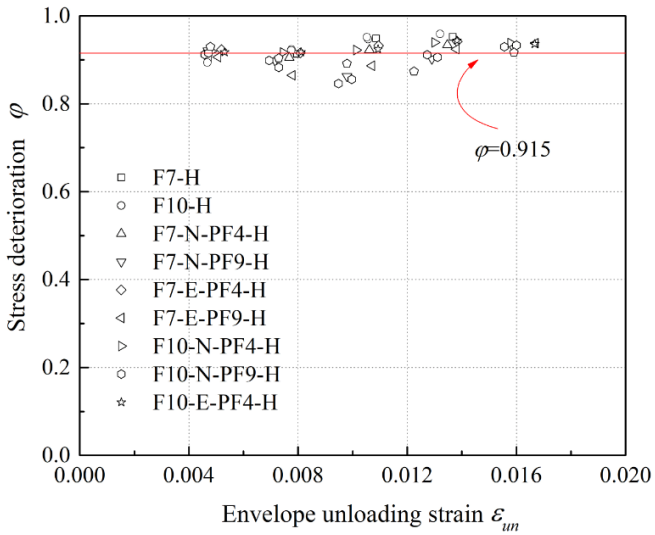

Fig. 17 Stress deterioration ratios at different unloading strains for the tested specimens

4.7 Reloading curves

The typical reloading path is characterized by a linear first portion and nonlinear second portion for FRP-confined concrete as shown in Fig. 9. For existing reloading models as presented in Table 6, Lam and Teng's model [29]

and Yu et al.'s model [30] adopt the linear relation between the reloading strain ε_{re} (which is also the plastic strain ε_{pl} of the previous unloading cycle) and the reference strain ε_{ref} (which is also the unloading strain ε_{un} of the previous unloading cycle), while non-linear relation is considered with the corresponding equations after the reference strain ε_{ref} until the reloading curve meets the envelope curve or the reloading curve reaches the next unloading point. Li et al.'s reloading model [33] adopts the four-parameter function, describing the nonlinear curve with two approximately linear portions and a nonlinear transition portion in between. These models are in line with the reloading behavior of FRP-confined concrete as shown in Fig. 9. By contrast, the models proposed by Wang et al. [31] and Hany et al. [32] adopt the linear equations from the reloading point to the envelope curve and omit the nonlinear transition portion, which is not consistent with the typical reloading behavior of FRP-confined concrete column as shown in Fig. 9.

For FRP-concrete double tube composite columns, an obvious stiffness difference can be observed at the initial stage for each reloading curve as shown in Fig. 12, which is different from the reloading curve for normal FRP-confined concrete as shown in Fig. 9. The axial load increases relatively slowly at the beginning and then increases faster with the development of axial strain. It is believed that during the beginning reloading stage, FRP tubes with the linear stress-strain behavior are fully in compression, while concrete is not fully compressed. As discussed in Sections 4.4 and 4.5 of this paper, in the unloading stage, the concrete stress will be zero when reaching the plastic strain $\varepsilon_{pl,1}$ and is assumed to be unchanged till reaching the plastic strain $\varepsilon_{pl,2}$ of the composite column. Therefore, the unloading stiffness between $\varepsilon_{pl,1}$ and $\varepsilon_{pl,2}$ is equal to the unloading stiffness of the FRP tubes. From the cyclic test curves, it can be observed that the reloading stiffness between $\varepsilon_{pl,2}$ and $\varepsilon_{pl,1}$ in the reloading curve is larger than the unloading stiffness between $\varepsilon_{pl,1}$ and $\varepsilon_{pl,2}$ in the unloading curve, but lower than the reloading stiffness after $\varepsilon_{pl,1}$ in the reloading curve. This indicates that in the reloading process between $\varepsilon_{pl,2}$ and $\varepsilon_{pl,1}$, not only the FRP tubes, but also the core concrete and ring concrete are under compression as well to contribute to the reloading stiffness to some extent.

For simplicity, two linear stages with different reloading stiffnesses are assumed between reloading strain ε_{re} and the reference strain ε_{ref} for the core concrete and ring concrete in the FRP-concrete double tube composite column, as shown in Fig. 12. $E_{re,1}$ is adopted as the slope of the reloading stress-strain curve for core concrete or ring

concrete in the range between $\varepsilon_{pl,2}$ and $\varepsilon_{pl,1}$, while $E_{re,2}$ is adopted as the slope of the reloading stress-strain curve for core concrete or ring concrete in the range between $\varepsilon_{pl,1}$ and ε_{ref}. Similar to that for the unloading curve in which the load carried by the FRP tubes decreases linearly from the unloading strain ε_{un} to the plastic strain $\varepsilon_{pl,2}$, the load carried by the FRP tubes is assumed to increase linearly from the plastic strain $\varepsilon_{pl,2}$ to the next unloading strain.

Test axial loads corresponding to the axial strain $\varepsilon_{pl,1}$ in the reloading curve were collected for each double tube composite column. The load F_{con} carried by core concrete and ring concrete can be determined by subtracting the load F_{frp} carried by the FRP tubes from the total axial load F_{total}. Therefore, the following equations can be obtained to calculate $E_{re,1,core}$ and $E_{re,1,ring}$ for core concrete and ring concrete:

$$E_{re,1,core} = \gamma E_{c,core} = \frac{(F_{total} - F_{frp})}{(E_{c,core}A_{core} + E_{c,ring}A_{ring})(\varepsilon_{pl,1} - \varepsilon_{pl,2})} E_{c,core} \tag{19}$$

$$E_{re,1,ring} = \gamma E_{c,ring} = \frac{(F_{total} - F_{frp})}{(E_{c,core}A_{core} + E_{c,ring}A_{ring})(\varepsilon_{pl,1} - \varepsilon_{pl,2})} E_{c,ring} \tag{20}$$

in which $E_{c,core}$ and $E_{c,ring}$ are the elastic moduli of core concrete and ring concrete, A_{core} and A_{ring} are the sectional areas of core concrete and ring concrete. γ is regarded as the reduction factor between $E_{re,1}$ and concrete elastic modulus E_c. The reduction factor γ is presented in Fig. 18. It is shown that γ is nearly a constant and is irrelevant to the plastic strain $\varepsilon_{pl,1}$. Therefore, it can be regressed that $\gamma = 0.13$ based on the current obtained test results.

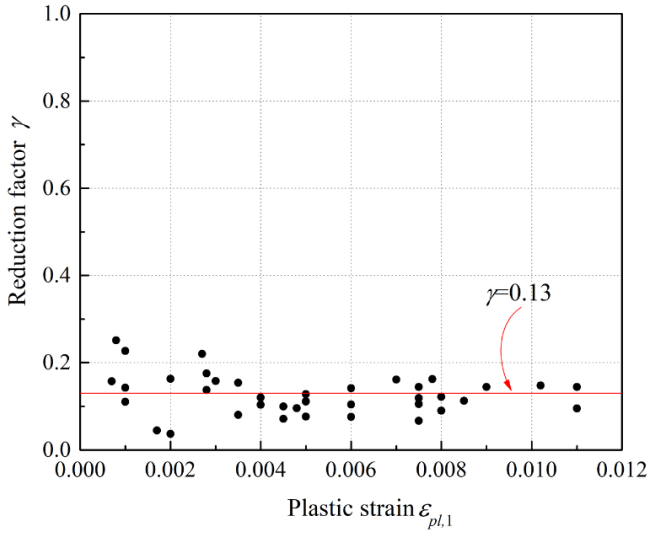

Fig. 18 Elastic modulus reduction factor at different plastic strains $\varepsilon_{pl,1}$

When $E_{re,1}$ is determined, the axial stresses $\sigma_{pl,1,core}$ and $\sigma_{pl,1,ring}$ in core concrete and ring concrete at the axial strain of $\varepsilon_{pl,1}$ in the reloading curve can then be calculated as follows:

$$\sigma_{pl,1,core} = E_{re,1,core}(\varepsilon_{pl,1} - \varepsilon_{pl,2}) \tag{21}$$

$$\sigma_{pl,1,ring} = E_{re,1,ring}(\varepsilon_{pl,1} - \varepsilon_{pl,2}) \tag{22}$$

With the stress deterioration φ determined in Section 4.6 of this paper, the new axial stress σ_{new} of core concrete and ring concrete at the strain ε_{ref} (which is also the unloading strain ε_{un} of the previous unloading cycle) can be calculated. Therefore, the slope $E_{re,2}$ can be calculated with the following equations for core concrete and ring concrete:

$$E_{re,2,core} = \frac{\sigma_{new,core} - \sigma_{pl,1,core}}{\varepsilon_{un} - \varepsilon_{pl,1}} = \frac{\varphi\sigma_{un,core} - \sigma_{pl,1,core}}{\varepsilon_{un} - \varepsilon_{pl,1}} \tag{23}$$

$$E_{re,2,ring} = \frac{\sigma_{new,ring} - \sigma_{pl,1,ring}}{\varepsilon_{un} - \varepsilon_{pl,1}} = \frac{\varphi\sigma_{un,ring} - \sigma_{pl,1,ring}}{\varepsilon_{un} - \varepsilon_{pl,1}} \tag{24}$$

Following Eq. (1), the axial loads at the corresponding axial strains of $\varepsilon_{pl,1}$ and ε_{ref} (ε_{un}) in the reloading curve can be obtained for the FRP-concrete double tube composite column.

For the existing reloading models presented in Table 6, Lam and Teng's model [29] and Yu et al.'s model [30], which are with the same equations, can be adopted to predict the nonlinear portion after the reference strain ε_{ref} in the reloading curve. Since Wang et al.'s model [31] and Hany et al.'s model [32] cannot describe the nonlinear portion, and Li et al.'s model [33] describes the whole reloading curve starting from the reloading strain ε_{re} and cannot be used together with the above proposed bi-linear portion from reloading strain ε_{re} to the reference strain ε_{ref}, they are not used for the reloading prediction in the current study.

4.8 Evaluation of proposed cyclic load-strain model

In Section 4.3 of this paper, modified envelope model based on Lam and Teng's monotonic stress-strain model [44] was developed for FRP-confined HSC, NC and ECC with the newly proposed equations for the ultimate conditions. In Section 4.4 of this paper, five existing unloading models were evaluated and exhibited good performance on the predictions of the unloading behavior for the composite column. In Sections 4.5 and 4.6 of this paper, equations of plastic strains and stress deterioration were proposed based on the test data obtained in this

study. In Sections 4.7 of this paper, two linear stages with different reloading stiffnesses were firstly proposed to describe the bi-linear load-strain behavior between reloading strain ε_{re} and the reference strain ε_{ref}. Lam and Teng's model [29] were then selected to predict the nonlinear portion after ε_{ref} in the reloading curve. Therefore, the cyclic load-strain model for the composite column can be developed with the aforementioned components and the load prediction equation Eq. (1). It is noted that Lam and Teng's unloading model [29] is used in this proposed model due to its good performance as shown in Fig. 13, as well as to keep consistent with the adopted Lam and Teng's reloading model [29] for the nonlinear portion.

Predicted cyclic load-strain curves by the proposed model are plotted and compared with test curves in Fig. 19. In the calculation of the predicted curves, except for the actual unloading strain for each loading cycle, all the other parameters used are based on the newly developed or selected models and equations. It is observed from Fig. 19 that close agreements between the predicted curves and test curves can be obtained, indicating the good performance of the proposed cyclic load-strain model on predicting the compressive behavior of the FRP-concrete double tube composite column under cyclic compression.

In the current study, the effect of biaxial stress state in the outer filament winding FRP tube on the lateral confinement effectiveness was not considered in the modeling for simplification, due to the obviously lower axial compressive stiffness than the hoop tensile stiffness. This effect could be considered in future studies to improve the model accuracy, especially when the confining FRP tube has a relatively large axial stiffness. Meanwhile, it is worth noting that only envelope unloading/reloading cycles (in which the unloading path occurs from the point on the envelope curve) are investigated in the current study for FRP-concrete double tube composite columns. Design equations for considering the cumulative effect on the plastic strains and stress deteriorations for composite columns under internal unloading/reloading cycles (in which the unloading path occurs from the point on the reloading curve under the envelope curve) may need to be developed based on the corresponding test data in future studies.

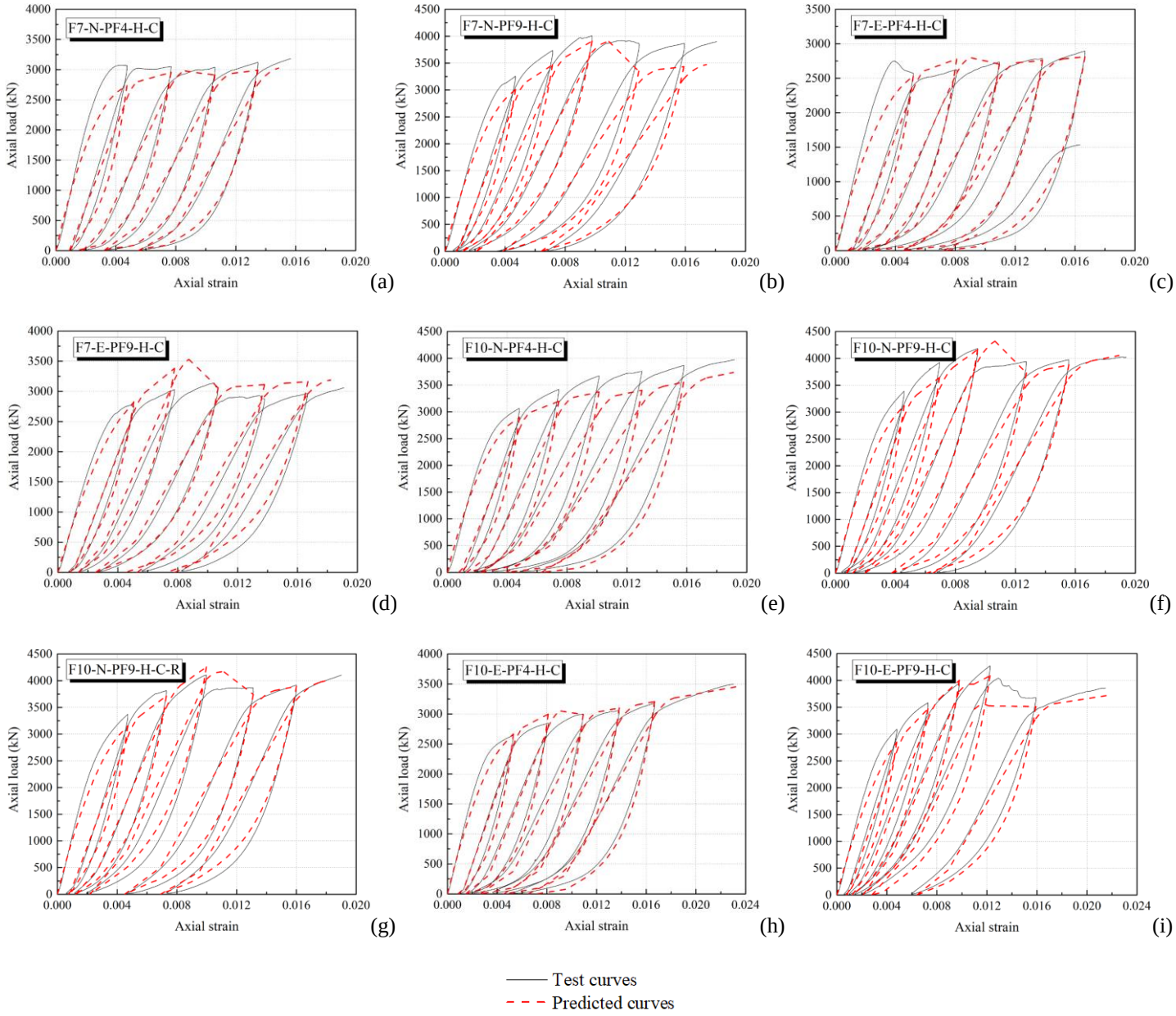

Fig. 19 Predictions of axial load-axial strain curves for FRP-concrete double tube composite columns

5. Conclusions

This paper presented the experimental investigation on the cyclic compressive behavior of the FRP-concrete double tube composite columns. Failure modes, load-strain responses and hoop strain behavior were discussed. Envelope curves, unloading/reloading curves, plastic strain and stress deterioration behavior were analyzed, followed by the development of the cyclic load-strain model for the FRP-concrete double tube composite column. The following conclusions can be drawn within the current scope of this study:

(1) All the specimens failed by outer filament winding FRP tube rupture. Similar to the monotonically loaded specimens, compressive behavior of the FRP-concrete double tube composite columns under cyclic

compression can be enhanced with the ultimate load capacity and the ultimate axial strain increased by 1.1 – 36.1% and 10.6 – 63.1%, respectively, compared to the counterpart FRP-confined HSC columns. The improved ultimate axial strain of the double tube composite column indicates the good deformability behavior.

(2) Load carrying capacity of the double tube composite column increases with the increase of the inner pultruded FRP tube thickness. Compared with specimens with NC as the ring concrete, the specimens with ECC ring can develop larger ultimate axial strain and relatively lower load carrying capacity.

(3) For both axial load-axial strain response and hoop strain-axial strain response, the envelope curves of specimens under cyclic compression are close to the curves of specimens under monotonic compression. The cyclically loaded specimens can generally develop more uniform hoop strain distributions than the counterpart monotonically loaded specimens, which also results in the delayed column failure.

(4) With the proposed equation of axial load, load-strain curves of the FRP-concrete double tube composite columns can be generated based on the stress-strain curves of FRP-confined HSC, NC and ECC. Lam and Teng's monotonic stress-strain model [44] was modified with the newly proposed equations of ultimate conditions. It can provide close predictions on the load-strain behavior for the monotonically loaded columns and can be used to predict the envelope curves for the cyclically loaded columns.

(5) Existing unloading models were evaluated and selected to predict the unloading curves for the tested columns. Bi-linear first portion was newly proposed with the nonlinear second portion predicted by Lam and Teng's model [29] to predict the reloading behavior. Meanwhile, new equations of plastic strains and stress deterioration were proposed based on the test results obtained in this study.

(6) Cyclic load-strain model was proposed with the aforementioned components. Close agreements between the predicted curves and the test curves demonstrate the good performance of the proposed model on predicting the cyclic compressive behavior of the FRP-concrete double tube composite columns.

CRediT authorship contribution statement

Shuai Li: Investigation, Writing - original draft. **Tak-Ming Chan:** Writing - review & editing, Funding acquisition, Supervision. **Ben Young:** Writing - review & editing, Funding acquisition, Supervision.

Declaration of Competing Interest

The authors declare that they have no known competing financial interests or personal relationships that could have appeared to influence the work reported in this paper.

Acknowledgement

The research work presented in this paper was supported by the Research Grants Council of the Hong Kong Special Administrative Region, China – Theme-based Research Scheme (Project No. T22-502/18-R).

References

[1] Zhu JY, Lin G, Teng JG, Chan TM, Zeng JJ, Li LJ. FRP-Confined square concrete columns with section curvilinearization under axial compression. J Compos Constr 2020;24(2):04020004.

[2] Ho JCM, Ou XL, Chen MT, Wang Q, Lai MH. A path dependent constitutive model for CFFT column. Eng Struct 2020;210:110367.

[3] Li S, Chan TM, Young B. Mechanical analysis and finite element modeling of FRP-ECC-HSC composite stub column under axial compression. J Build Eng 2022;62:105212.

[4] Sirach N, Smith ST, Yu T, Mostafa A. Experimental study on the confinement of concrete cylinders with large rupture-strain FRP composites. J Compos Constr 2021;25(4):04021026.

[5] Bai YL, Dai JG, Mohammadi M, Lin G, Mei SJ. Stiffness-based design-oriented compressive stress-strain model for largerupture-strain (LRS) FRP-confined concrete. Compos Struct 2019;223:110953.

[6] Yang JQ, Feng P. Analysis-oriented model for FRP confined high-strength concrete: 3D interpretation of path dependency. Compos Struct 2021;278:114695.

[7] Ozbakkaloglu T, Lim JC, Vincent T. FRP-confined concrete in circular sections: Review and assessment of stress–strain models. Eng Struct 2013;49:1068–1088.

[8] Li S, Chan TM, Young B. Experimental investigation on axial compressive behavior of novel FRP-ECC-HSC composite short column. Compos Struct 2023;303:116285.

[9] Wei Y, Bai J, Zhang Y, Miao K, Zheng K. Compressive performance of high-strength seawater and sea sand concrete-filled circular FRP-steel composite tube columns. Eng Struct 2021;240:112357.

[10] Zeng JJ, Zheng YW, Liu F, Guo YC, Hou C. Behavior of FRP ring-confined CFST columns under axial compression. Compos Struct 2021;257:113166.

[11] Zhang B, Yu T, Teng JG. Behavior and modelling of FRP-concrete-steel hybrid double-skin tubular columns under repeated unloading/reloading cycles. Compos Struct 2021;258:113393.

[12] Wang Y, Zhong Y, Wan B, Zhang B, Wei Z, Bai Y. Axial compressive behavior and modeling of fiber-reinforced polymer-concrete-steel double-skin tubular stub columns with a rectangular outer tube and an elliptical inner tube. Eng Struct 2022;260:114222.

[13] Zeng JJ, Lv JF, Lin G, Guo YC, Li LJ. Compressive behavior of double-tube concrete columns with an outer square FRP tube and an inner circular high-strength steel tube. Constr Build Mater 2018;184:668-680.

[14] Li YL, Zhao XL. Hybrid double tube sections utilising seawater and sea sand concrete, FRP and stainless steel. Thin-Walled Struct 2020;149:106643.

[15] Zeng JJ, Ye YY, Guo YC, Lv JF, Ouyang Y, Jiang C. PET FRP-concrete-high strength steel hybrid solid columns with strain-hardening and ductile performance: Cyclic axial compressive behavior. Compos Part: B 2020;190:107903.

[16] Ye YY, Zhu DH, Zeng JJ, Lin G, Wang WQ. Rectangular double-tube concrete columns with an internal elliptical high-strength steel tube: Concept and behavior. Eng Struct 2020;216:110742.

[17] Li S, Chan TM, Young B. Compressive behavior and analysis-oriented model of FRP-confined engineered cementitious composite columns. Eng Struct 2022;270:114869.

[18] Zeng JJ, Feng P, Dai JG, Zhuge Y. Development and behavior of novel FRP-UHPC tubular members. Eng Struct 2022;266:114540.

[19] Cao S, Wu C, Wang W. Behavior of FRP confined UHPFRC-filled steel tube columns under axial compressive loading. J Build Eng 2020;32:101511.

[20] Lam L, Huang L, Xie JH, Chen JF. Compressive behavior of ultra-high performance concrete confined with FRP. Compos Struct 2021;274:114321.

[21] Li S, Chan TM, Young B. Behavior of GFRP-concrete double tube composite columns. Thin-Walled Struct 2022;178:109490.

[22] Li YL, Zhao XL, Singh Raman RK, Al-Saadi S, Tests on seawater and sea sand concrete-filled CFRP, BFRP and stainless steel tubular stub columns. Thin-Walled Struct 2016;108:163-184.

[23] Teng JG, Xiang Y, Yu T, Fang Z. Development and mechanical behaviour of ultra-high-performance seawater sea-sand concrete. Adv Struct Eng 2019; 22(14):3100-3120.

[24] Bai YL, Mei SJ, Li P, Xu J. Cyclic stress-strain model for large-rupture strain fiber-reinforced polymer (LRS FRP)-confined concrete. J Build Eng 2021;42:102459.

[25] Zeng JJ, Ye YY, Guo YC, Lv JF, Ouyang Y, Jiang C. PET FRP-concrete-high strength steel hybrid solid columns with strain-hardening and ductile performance: Cyclic axial compressive behavior. Compos Part B 2020;190:107903.

[26] Zhou JK, Lin G, Teng JG. Compound concrete-filled FRP tubular columns under cyclic axial compression. Compos Struct 2021;275:114329.

[27] Shao Y, Zhu Z, Mirmiran A. Cyclic modeling of FRP-confined concrete with improved ductility, Cement Concr Compos 2006;28(10):959–968.

[28] Lam L, Teng JG, Cheung JG, Xiao Y. FRP-confined concrete under axial cyclic compression. Cem Concr Compos 2006;28(10):949–58.

[29] Lam L, Teng JG. Stress–strain model for FRP-confined concrete under cyclic axial compression, Eng Struct 2009;31:308–321.

[30] Yu T, Zhang B, Teng JG. Unified cyclic stress–strain model for normal and high strength concrete confined with FRP. Eng Struct 2015;102:189-201.

[31] Wang Z, Wang D, Smith ST, Lu D. Experimental testing and analytical modeling of CFRP-confined large circular RC columns subjected to cyclic axial compression. Eng Struct 2012;40:64-74.

[32] Hany NF, Hantouche EG, Harajli MH. Axial stress-strain model of CFRP-confined concrete under monotonic and cyclic loading. J Compos Constr 2015;19(6):04015004.

[33] Li P, Wu YF, Zhou Y, Xing F. Cyclic stress-strain model for FRP-confined concrete considering post-peak softening. Compos Struct 2018;201:902-915.

[34] Zhang Y, Wei Y, Miao K, Li B. A novel seawater and sea sand concrete-filled FRP-carbon steel composite tube column: Cyclic axial compression behaviour and modelling. Eng Struct 2022;252:113531.

[35] Zhang Y, Wei Y, Zhao K, Ding M, Wang L. Analytical model of concrete-filled FRP-steel composite tube columns under cyclic axial compression. Soil Dyn Earthq Eng 2020;139:106414.

[36] Chen G, Wang Y, Cai G, Si Larbi A, Wan B, Hao Q. Performance and modeling of FRP-steel dually confined reinforced concrete under cyclic axial loading. Compos Struct 2022;300:116076.

[37] Li VC. On engineered cementitious composites (ECC). J Adv Concr Technol 2003;1(3):215–30.

[38] Zhu JX, Xu LY, Huang BT, Weng KF, Dai JG. Recent developments in Engineered/Strain-Hardening Cementitious Composites (ECC/SHCC) with high and ultra-high strength. Constr Build Mater 2022;342:127956.

[39] Zhang B, Yu T, Teng JG. Behavior of concrete-filled FRP tubes under cyclic axial compression. J Compos Constr 2015;19(3):04014060.

[40] Dang Z, Feng P, Yang JQ, Zhang Q. Axial compressive behavior of engineered cementitious composite confined by fiber-reinforced polymer. Compos Struct 2020;243:112191.

[41] Yuan WY, Han Q, Bai YL, Du XL, Yan ZW. Compressive behavior and modelling of engineered cementitious composite (ECC) confined with LRS FRP and conventional FRP. Compos Struct 2021;272:114200.

[42] Zhang B, Teng JG, Yu T. Compressive behavior of double-skin tubular columns with high-strength concrete and a filament-wound FRP tube. J Compos Constr 2017;21(5):04017029.

[43] Xie J, Wang Z, Yan JB. Axial compression behaviours of seawater and sea sand concrete-filled GFRP stub tubes at arctic low temperatures. Thin-Walled Struct 2022;170:108566.

[44] Lam L, Teng JG. Design-oriented stress-strain model for FRP-confined concrete. Constr Build Mater 2003;17(6):471-489.

[45] Yu T, Teng JG, Wong YL. Stress-strain behavior of concrete in hybrid double-skin tubular columns. J Struct Eng 2010;136(4):379-389.

[46] Liao JJ, Zeng JJ, Jiang C, Li JX, Yuan JS. Stress-strain behavior and design-oriented model for FRP spiral strip-confined concrete. Compos Struct 2022;293:115747.

[47] Teng JG, Jiang T, Lam L, Luo YZ. Refinement of a design-oriented stress–strain model for FRP-confined concrete. J Compos Constr 2009;13(4):269-278.

[48] Liao J, Zeng JJ, Gong QM, Quach WM, Gao WY, Zhang L. Design-oriented stress-strain model for FRP-confined ultra-high performance concrete (UHPC). Constr Build Mater 2022;318:126200.

[49] Chen G, Wang Y, Yu T, Wan B, Zhang B, Liu Q. Behavior and design-oriented model for elliptical FRP-confined concrete under axial compression. Eng Struct 2021;249:113387.

[50] Concrete Society, Design guidance for strengthening concrete structures with fibre composite materials, Technical Rep. No. 55, 3rd Ed., Crowthorne, Berkshire, U.K. 2012.

[51] American Concrete Institute ACI, Guide for the design and construction of externally bonded FRP systems for strengthening concrete structures, ACI-440 2R, Farmington Hills, Mich. 2017.

[52] Yu T, Zhang B, Cao YB, Teng JG. Behavior of hybrid FRP-concrete-steel double-skin tubular columns subjected to cyclic axial compression. Thin-Walled Struct 2012;61:196-203.